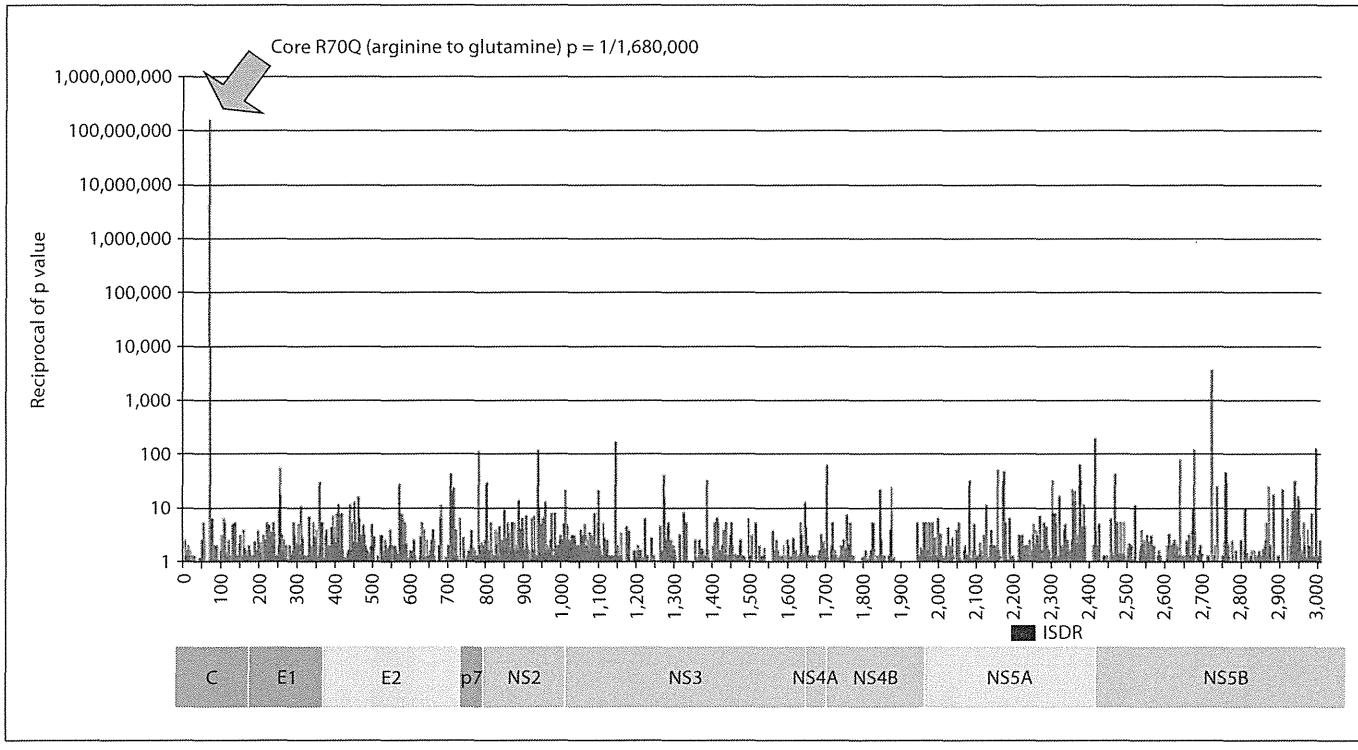

Fig. 2. Reciprocal of p value for single amino acid difference along the whole HCV sequence for non-EVR versus others.

comparing amino acids between the non-EVR patients and the others, remarkable differences were clustered in a single amino acid polymorphism in the core 70. Recent studies have proven that the initial viral response at week 4 and week 12 of the PEG-IFN/RBV therapy could be a useful predictor of the final outcome, indicating that the present findings are important for predicting treatment outcome and individualizing the treatment regimen for each patient as well as understanding the mechanism of diverse response to PEG-IFN/RBV therapy.

ISDR was first identified as the region significantly related to SVR in the era of IFN monotherapy in Japanese patients [3, 4]. 'Mutant type', meaning 4 or more mutations in the region, was associated with high SVR rate, while the rate was low in the 'intermediate type' (1–3 mutations) and wild type (no mutation). Though there were controversies as to the predictive value of ISDR, since studies in Europe and in North America did not necessarily reproduce evident correlation between ISDR and SVR, a recent meta-analysis proved its value by demonstrating a clear relationship all over the world, even in Western countries [5]. The present study reproduced the significance of ISDR in PEG-IFN/RBV therapy. Mutations in ISDR make HCV highly sensitive to IFN, leading to RVR. Current guidelines indicate that RVR patients with low viral load before treatment can be treated with 24 weeks instead of the standard 48 weeks of therapy. Since most ISDR mutant patients show low viral loads, these easy-to-treat patients in genotype 1b should be mainly infected with HCV with ISDR mutations, suggesting ISDR genotyping would identify the patients treatable with the abbreviated regimen.

On the other hand, in the present study, the polymorphism of core 70 was extracted as the most significant position to determine poor virological response in 12 weeks (non-EVR). The contribution of core region amino acid polymorphism in resistance to (PEG-)IFN/RBV therapy was previously reported by Akuta et al. [6], who first found that the polymorphisms in a combination of core 70 and 91 were closely related to the final outcome. The importance of core 70 polymorphism alone, however, was considered rather weak in their study for its smaller p value. Their end point was the final outcome of the treatment, which could be influenced by a variety of factors other than viral genetics, such as host factors (age, sex, fibrosis, body weight, etc.) and treatment (dose of

PEG-IFN/RBV). Further studies are needed to clarify the significance of the core mutations for final outcome of the treatment in the context of the HCV genome-wide analysis.

Different viral responses by polymorphisms in core 70 were also recently suggested in North American patients by Donlin et al. [7]. However, it was reported that the association with core 70 was weaker in their study. Very recently, the IL28B (interferon-lambda-3) gene polymorphism has been found to be closely associated with treatment response in patients in the United States, European Union and Japan by human genome-wide analysis [8–10]. The favorable IL28B genotype is found most frequently in Asian patients, second in European-Americans, and least in African-Americans, indicating that a well-known racial difference in treatment efficacy can be explained by the IL28B polymorphism. The interaction between viral and human genome polymorphisms should be studied further with regard to the treatment response.

Conclusion

HCV genome-wide analysis with a large number of patients successfully revealed that core 70 and NS5A are the most important factors determining the virological kinetics during PEG-IFN/RBV therapy. Viral genome-wide analysis is a promising tool for elucidating the unknown viral factors for different pathological pictures, such as disease progression.

Disclosure Statement

Supported in part by a Grant-in-Aid for Research on Hepatitis (grant ID H19-002) from the Ministry of Health, Labor, and Welfare, Japan. The authors report receiving grant support from Schering-Plough and Roche.

References

1 Neumann AU, Pianko S, Zeuzem S, Yoshida EM, Benhamou Y, Mishan M, et al: Positive and negative prediction of sustained virologic response at weeks 2 and 4 of treatment with albinterferon alfa-2b or peginterferon alfa-2a in treatment-naive patients with genotype 1, chronic hepatitis C. J Hepatol 2009; 51:21–28.

2 Lee SS, Ferenci P: Optimizing outcomes in patients with hepatitis C virus genotype 1 or 4. Antivir Ther 2008;13(suppl 1):9–16.

3 Enomoto N, Sakuma I, Asahina Y, Kurosaki M, Murakami T, Yamamoto C, et al: Comparison of full-length sequences of interferon-sensitive and resistant hepatitis C virus 1b: sensitivity to interferon is conferred by amino acid substitutions in the NS5A region. J Clin Invest 1995;96:224–230.

4 Enomoto N, Sakuma I, Asahina Y, Kurosaki M, Murakami T, Yamamoto C, et al: Mutations in the nonstructural protein 5A gene and response to interferon in patients with chronic hepatitis C virus 1b infection. N Engl J Med 1996;334:77–81.

5 Pascu M, Martus P, Hohne M, Wiedenmann B, Hopf U, Schreier E, et al: Sustained virological response in hepatitis C virus type 1b infected patients is predicted by the number of mutations within the NS5A-ISDR: a meta-analysis focused on geographical differences. Gut 2004;53:1345–1351.

6 Akuta N, Suzuki F, Sezaki H, Suzuki Y, Hosaka T, Someya T, et al: Association of amino acid substitution pattern in core protein of hepatitis C virus genotype 1b high viral load and non-virological response to interferon-ribavirin combination therapy. Intervirology 2005;48:372–380.

7 Donlin MJ, Cannon NA, Yao E, Li J, Wahed A, Taylor MW, et al: Pretreatment sequence diversity differences in the full-length hepatitis C virus open reading frame correlate with early response to therapy. J Virol 2007; 81:8211–8224.

8 Ge D, Fellay J, Thompson AJ, Simon JS, Shianna KV, Urban TJ, et al: Genetic variation in IL28B predicts hepatitis C treatment-induced viral clearance. Nature 2009;461:399–401.

9 Suppiah V, Moldovan M, Ahlenstiel G: *IL28B* is associated with response to chronic hepatitis C interferon-α and ribavirin therapy. Nat Genet 2009;41:1100–1104.

10 Tanaka Y, Nishida N, Sugiyama M, Kurosaki M, Matsuura K, Sakamoto N, et al: Genome-wide association of *IL28B* with response to pegylated interferon-α and ribavirin therapy for chronic hepatitis C. Nat Genet 2009; 41:1105–1109.

BioSystems 99 (2010) 70–78

Contents lists available at ScienceDirect

BioSystems

journal homepage: www.elsevier.com/locate/biosystems

Reproducibility and usability of chronic virus infection model using agent-based simulation; comparing with a mathematical model

Jun Itakura[a,*], Masayuki Kurosaki[a], Yoshie Itakura[a], Sinya Maekawa[b], Yasuhiro Asahina[a], Namiki Izumi[a], Nobuyuki Enomoto[b]

[a] Division of Gastroenterology and Hepatology, Musashino Red Cross Hospital, 1-26-1 Kyonan-cho, Musashino-shi, Tokyo 180-8610, Japan
[b] First Department of Internal Medicine, Faculty of Medicine, University of Yamanashi, 1110, Shimogatou, Chuou-shi, Yamanashi 409-3898, Japan

ARTICLE INFO

Article history:
Received 30 June 2009
Received in revised form 27 August 2009
Accepted 6 September 2009

Keywords:
Agent-based model
Virus infectious disease

ABSTRACT

We created agent-based models that visually simulate conditions of chronic viral infections using two software. The results from two models were consistent, when they have same parameters during the actual simulation. The simulation results comprise a transient phase and an equilibrium phase, and unlike the mathematical model, virus count transit smoothly to the equilibrium phase without overshooting which correlates with actual biology in vivo of certain viruses. We investigated the effects caused by varying all the parameters included in concept; increasing virus lifespan, uninfected cell lifespan, uninfected cell regeneration rate, virus production count from infected cells, and infection rate had positive effects to the virus count during the equilibrium period, whereas increasing the latent period, the lifespan-shortening ratio for infected cells, and the cell cycle speed had negative effects. Virus count at the start did not influence the equilibrium conditions, but it influenced the infection development rate. The space size had no intrinsic effect on the equilibrium period, but virus count maximized when the virus moving speed was twice the space size. These agent-based simulation models reproducibly provide a visual representation of the disease, and enable a simulation that encompasses parameters those are difficult to account for in a mathematical model.

1. Introduction

All viruses need hosts as a basis for their life. When a virus enters the host body, it invades cells and uses both its own enzymes and those of the host cells to replicate. Host cells infected by viruses launch a self-defense system known as the innate immune system (See and Wark, 2008; Naniche, 2009), which inhibits viral replication and uses the human leukocyte antigen system and cytokines to elicit an immune response. Immune cells that have received signals from host cells activate other immune cells, neutralize viruses in the serum by means of antibodies, and prevent the virus from replicating and proliferating by destroying or curing host cells. Viral infection is a disorder based on the interactions between viruses and cells.

The power relationship between these agents changes along with the progression of the disease. In the very early stages of infection, as the host defense mechanisms are immature, the virus has the ability to overwhelm the host cells, actively replicate, and proliferate. Subsequently, as the capacity of the immune system improves, the speed of viral proliferation drops and the virus count reaches a peak. Infected host cells begin to be disrupted by the immune system or virus particles, and symptoms appear as a result. If the immune system is stronger than the virus, then the viral counts decline, and, in transient viral disorders, the virus is finally eliminated and the host recovers. In chronic viral disorders, however, the power relationship between the virus and host cells reaches equilibrium, and a long-term power balance is maintained with the virus count reaching a plateau.

Mathematical models have been proposed to study the dynamics of such viral disorders, and are regarded as being of value in understanding this phenomenon (Ho et al., 1995; Nowak et al., 1996; Neumann et al., 1998). However, these models are difficult to understand for clinicians, and their applicability is somewhat limited in everyday practice. In clinical research, measurements of viral dynamics in patients for short duration have been made for human

Abbreviations: HIV, human immunodeficiency virus; HBV, hepatitis B virus; HCV, hepatitis C virus.

* Corresponding author. Tel.: +81 422 32 3111; fax: +81 422 32 9551.
E-mail address: jitakura@musashino.jrc.or.jp (J. Itakura).

0303-2647/$ – see front matter © 2009 Elsevier Ireland Ltd. All rights reserved.
doi:10.1016/j.biosystems.2009.09.001

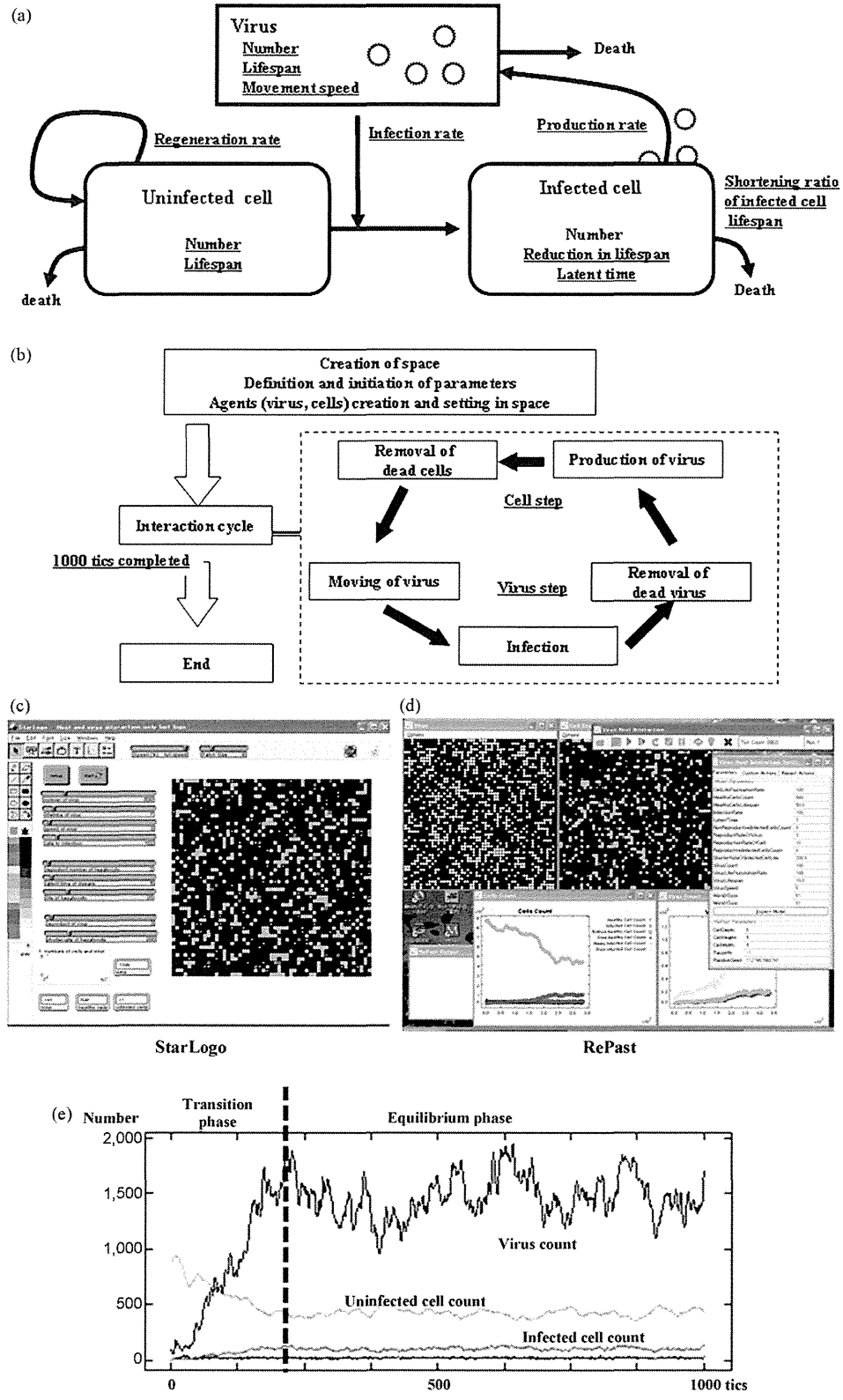

Fig. 1. Simulation design and an example of simulation results. (a) Model concept. Viruses, uninfected cells, and infected cells were treated as agents, and parameters were set for each of these and for interactions between agents (underlined). (b) Flowchart of the program. After preparing the simulation, we entered the interaction cycle, in which virus steps (such as movement) and cell steps were repeated. One cycle was counted as 1 tic, and the simulation concluded after 1000 tics. (c and d) Simulation screen using (c) StarLogo and (d) RePast. Yellow circles are viruses, green squares are uninfected cells, and orange and red indicate infected cells, with orange indicating the latent period. In StarLogo, all the agents are shown on the same screen, but in RePast, viruses and cells are shown in separate windows. (e) Example of a simulation chart in StarLogo. After the start of simulation the virus count and infected cell count increase while the uninfected cell count decreases, with equilibrium state reached after a certain number of tics.

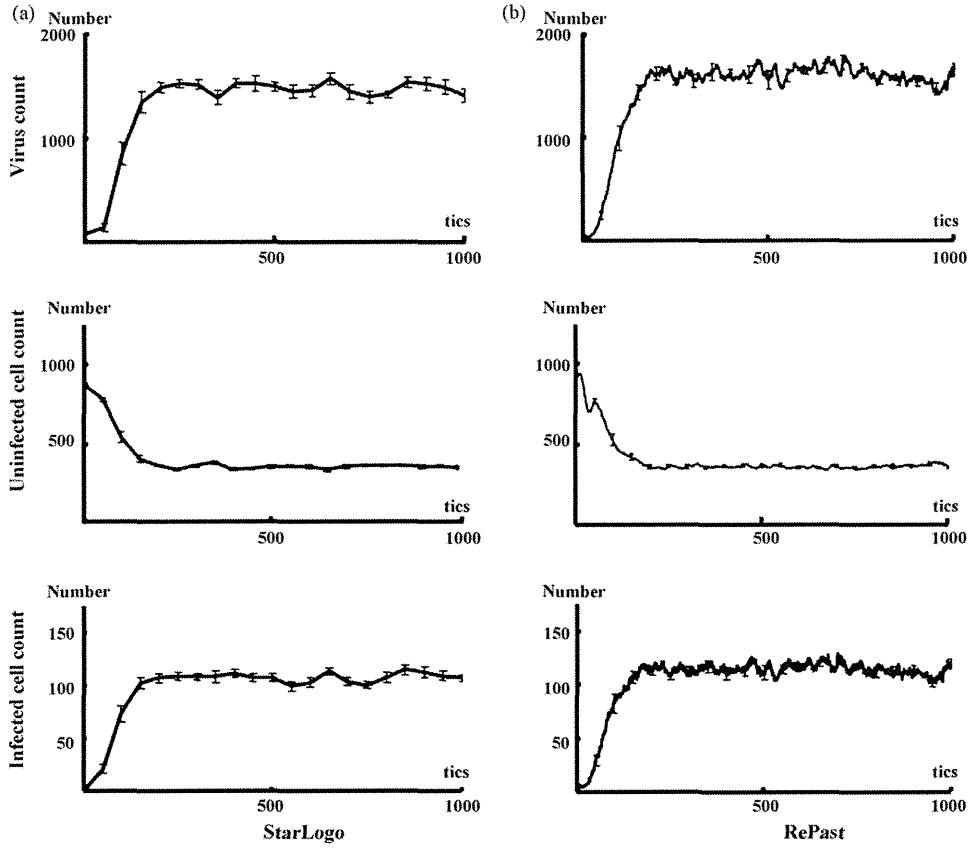

Fig. 2. Comparison of simulation results in (a) StarLogo and (b) RePast. The results were consistent when the parameters were made consistent. (Virus count [average ± SD]: StarLogo 1458.03 ± 173.1, RePast 1462.71 ± 178.8, $p = 0.94$. Uninfected cell count: 364.24 ± 30.4, 368.11 ± 33.4, $p = 0.83$. Infected cell count: 105.73 ± 13.0, 107.74 ± 13.0, $p = 0.24$. Unpaired Student's t-test.) Parameter values were set as follows: initial virus count, 100; uninfected cell count, 880; infected cell count, 0; virus speed of movement, 5 grids/tic; infection rate, 10%; uninfected cell regeneration rate, 1%; latent period, 3 tics; and virus reproduction rate, 5/cells/tic. The following parameter settings were taken from actual measurements: virus lifespan, 4.5 tics; uninfected cell lifespan, 49.8 tics; and infected cell lifespan, 6.7 tics.

immunodeficiency virus (HIV) (Ho et al., 1995), hepatitis B virus (HBV) (Nowak et al., 1996) and hepatitis C virus (HCV) (Neumann et al., 1998), and research is also underway on a range of models based on animal experiments and cell culture systems. As chronic viral disorders persist over long periods of time complete follow-up of viral dynamics is difficult. Furthermore, limitations of items that can be measured, such as the difficulty of measuring whole numbers of host cells, make it extremely difficult to investigate their consistency in mathematical models.

The recent ascend of dynamic-models owes much to advances in computers. Computer performance has improved markedly in recent years, not only in terms of their calculating capacity but also with regard to image displays, and models that offer a visual representation of viral disorders are now being reported (Gilbert and Bankes, 2002; Duca et al., 2007; Shapiro et al., 2008; Castiglione et al., 2007). One advantage of such visual models is that by providing a visual representation, they make understanding the disease status easy. Another benefit is that they enable parameters to be identified that are hidden as background noise in mathematical models. However, these models have some problems; it is difficult to prove the reproducibility of the simulation results derived from different languages or libraries, difficult to prove the validity of the model's concepts, and difficult to prove that the simulation results accurately reflect the reality. In this study, we created agent-based computer models that visually simulate the conditions of chronic viral infections using two software. The reproducibility of two agent-based computer models and the differences between agent-based models and the mathematical model were analyzed. This agent-based model enabled us to investigate how each parameter included in the concept affects the conditions of chronic viral infections.

2. Methods

2.1. Selection of Software

In this study, we used two different types of softwares: StarLogo version 2.0 (http://education.mit.edu/starlogo/) supplied by MIT Media Laboratory and Recursive Porous Agent Simulation Toolkit (RePast-3.0, http://repast.sourceforge.net/) supplied by the Argonne National Laboratory. StarLogo uses Logo, one of the simplest programming languages, and has a fixed graphical user interface. RePast is a library that uses Java, another programming language, which also has a fixed graphical user interface.

Logo is an assembly language, and StarLogo carries out processing sequentially. Java is an object-oriented language, and RePast has a faster processing speed than StarLogo. In addition, StarLogo has a number of stipulations to simplify simulations, such as parameters can only be set up to five decimal places and the simulation space is also fixed as 51 × 51 square grids. RePast, on the other hand, has fewer such restrictions. Thus, it offers a higher degree of freedom in program settings than StarLogo. Taking simulation space as an example, in spite of the restrictions imposed by the underlying operating system's image display system, any number of grids can be set and a hexagonal grid could also be chosen rather than a square one. However, users must stipulate and set all parameters themselves. This means that they must first declare the shape of the grid and the number of grids they will use to fill the simulation space. Java is also more difficult to learn than Logo, and debugging and correcting the program is also more difficult. Thus, it is difficult to judge whether or not the results agree with the planned simulation.

In effect, these two different types of softwares are polar opposites. It is simple to start a simulation in StarLogo, but producing results takes time and it is difficult to carry out more complex simulations. In RePast it is difficult to compose the program and judge whether or not the planned study has actually been achieved, but the

simulation itself takes only a short time to complete and there are lesser restrictions in the construction of a simulation model.

2.2. Concept for Modeling

We applied the basic virus–host interaction mathematical model to the agent-based simulation system with slight modifications. The mathematical model was used to describe the dynamics of HIV (Ho et al., 1995), HBV (Nowak et al., 1996), and HCV (Neumann et al., 1998) and the only agents involved were host cells and viruses, without the inclusion of immune cells. The effects of the immune system are expressed by varying parameters such as lifespan of host cells and viruses.

Fig. 1a illustrates the study concept. Viruses have the ability to infect healthy host cells (uninfected cells) and the infected cells produce new viruses. Both cells and viruses have definite lifespans, and the lifespan of infected cells is usually shorter than that of uninfected cells. Uninfected cells automatically regenerate within the space, whereas infected cells only arise due to infection of uninfected cells. Viruses also lack the ability to regenerate themselves and are only produced from infected cells.

2.3. Parameter Settings

In the present study, as the StarLogo settings are circumscribed, we limited the simulation space to 51 × 51 square grids. However, we made an exception here while investigating the effects of size of space on the simulation results. The numbers of viruses, uninfected cells, and infected cells could only be set before the start of the simulation. As described in the later, our simulation ran in cycles, with 1 cycle defined as 1 tic.

In mathematical simulation models, the death rate is required as a parameter. However, in our program we set lifespans for viruses and uninfected cells. These lifespans were not uniform, but were set to have a deviation of about 10%. The lifespan of cells was shortened by infection with ratio decided beforehand.

The infection ratio was meaningful only when an infected cell and a virus coincidentally occupied the same grid, and this was used to calculate the probability of the infection occurring in that situation. The virus production rate was set as the number of viruses produced by an infected cell during 1 tic. Infected cells could be set as a parameter indicating the latent period between the time of virus infection and the time of virus replication.

In order to emulate the tissue repair capacity, we set uninfected cell regeneration rate such that grids without any cells had a specified probability of producing uninfected cells on top of themselves. As a result, the more the cell count declined within a space the more regenerated uninfected cells were produced, whereas the number of regenerated cells declined as cell count increased.

The number of grids through which a virus could move in 1 tic was set as the speed of movement, and the direction of movement was set within a range of 90° toward the top of the simulation space. The program used a circulatory method of movement; when a virus arrived at the top of the space, it was translocated to the bottom, and moved again toward the top. Cells were fixed on the grid.

2.4. Simulation Flowchart

Fig. 1b shows a flowchart of the program. First, the simulation space was produced, after which each parameter was defined and the initial settings were made. Next the agents – viruses and uninfected and infected cells – were produced. The simulation cycle was as follows. Viruses moved to a new grid, and if an uninfected cell was present, this was infected with a probability based on the infection rate. The lifespan of the virus decreased, and viruses that had completed their lifespan and those that had caused an infection were removed from the space. Infected cells produced new viruses, the lifespans of both uninfected and infected cells decreased. Then, cells that had completed their lifespan were eliminated and a new cycle began. The program was set such that the simulation ended after this cycle had repeated 1000 times. This meant that one simulation was complete after 1000 tics.

2.5. Data Collection

The RePast model was programmed such that data for each tic was saved automatically as a text file at the end of the simulation. This text file could be opened by a database software. The StarLogo model was programmed to stop the simulation and collect data after every 50 tics.

2.6. Mathematical Model

In order to compare the results of this agent-based simulation, we used a viral infection mathematical model, which we improved as follows.

$$\frac{dT}{dt} = s[2601 - (T + I)] - dT - bVT \quad (1)$$

$$\frac{dI}{dt} = bVT - dI \quad (2)$$

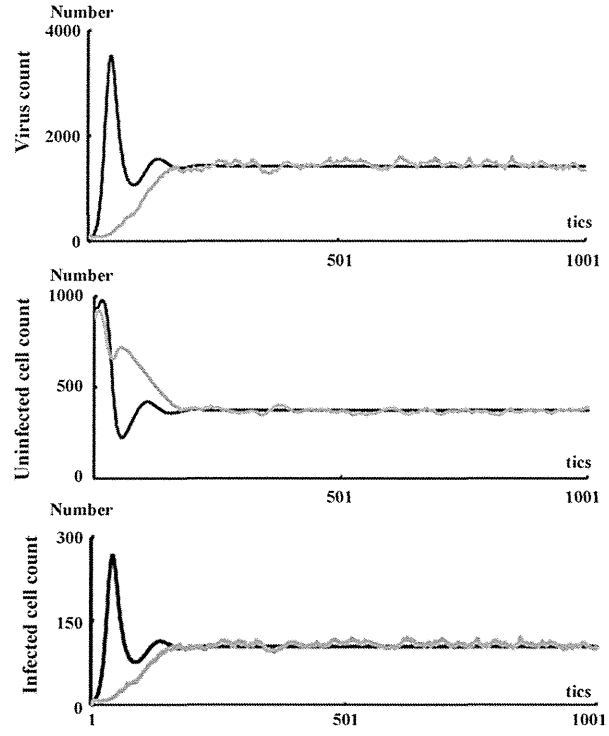

Fig. 3. Comparison of results of agent-based simulation and mathematical simulation. Both sets of results were consistent for the equilibrium phase, but differed in the shift in transition phase. Black line: mathematical model; grey line: results of simulation in RePast. Parameter values were set as follows: initial virus count, 100; uninfected cell count, 880; infected cell count, 0; virus speed of movement, 5 grids/tic; infection rate, 10%; uninfected cell regeneration rate, 1%; latent period, 3 tics; virus reproduction rate, 5/cells/tic; virus lifespan, 10 tics; uninfected cell lifespan, 50 tics; and cell lifespan-shortening ratio as a result of infection, 69%.

$$\frac{dV}{dt} = pI - cV \quad (3)$$

where, T is the uninfected cell count, I is the infected cell count, and V is the virus count. Uninfected cells are supplied to the space with a probability $s[2601 - (T+I)]$, as the number of grids in this agent-based simulation model was 2601 (51 × 51). The death rate of uninfected cells is d, the death rate of infected cells is δ, and the death rate of viruses is c. The infection rate is indicated by β. Viruses are released from infected cells at a probability p.

2.7. Statistical Analysis

Statistical analyses were performed by statistical tests using the program StatView 5.0 (SAS Institute Inc.). All tests of significance were two-tailed, with p values of <0.05 considered to be significant.

3. Results

3.1. Reproducibility of Chronic Viral Infection Disease Models Using Agent-based Simulation Methods

We constructed the chronic viral infection model with StarLogo library. Fig. 1c shows the simulation screen, and Fig. 1e shows one sample result. Immediately after the start of the simulation, the virus count temporarily dropped in accordance with the onset of an infection. Subsequently, the virus count started to increase with an increase in the infected cells and a decrease in the uninfected cells. After a certain number of tics (around 300 in this example), although the virus count, infected cell count, and uninfected cell count had some fluctuation, an equilibrium state was reached. We use the following descriptive terms in this paper: the transient phase is the period during which virus growth peaks, and the equilibrium phase is the period during which an equilibrium state is

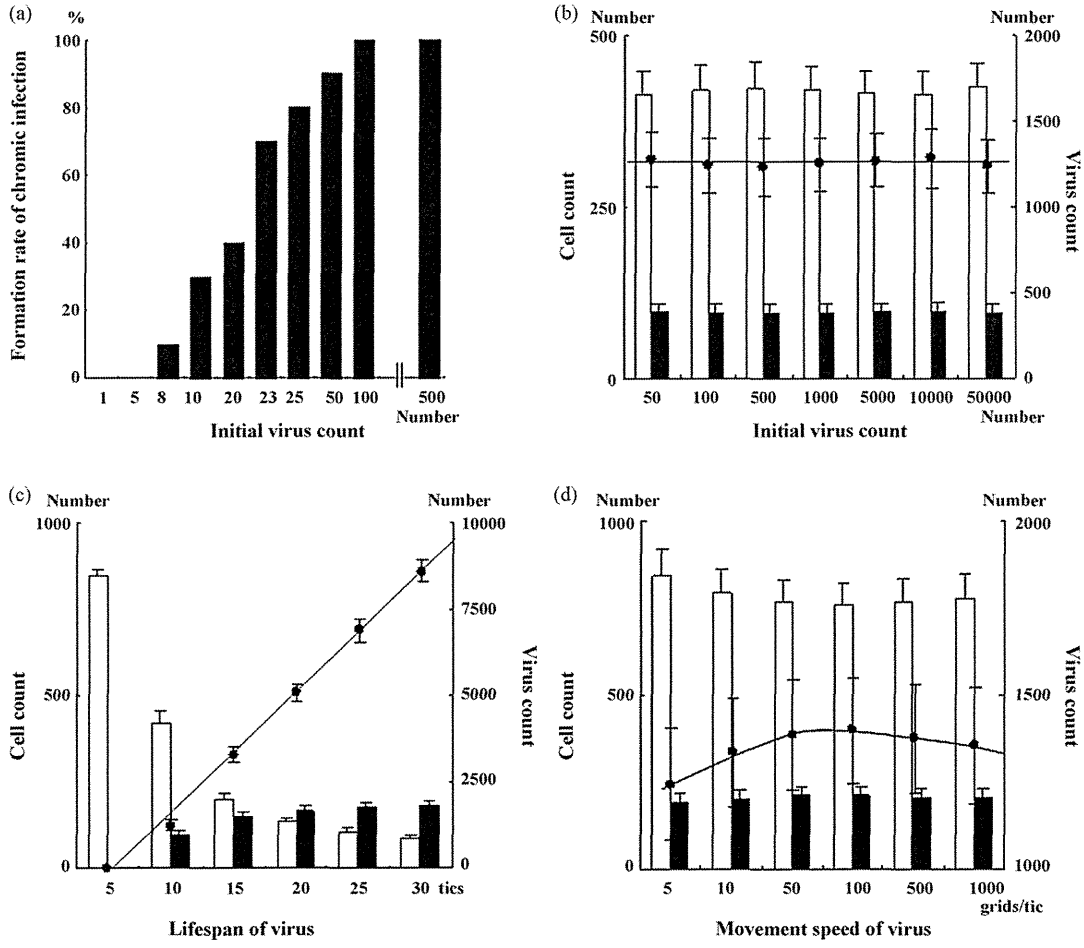

Fig. 4. *Effects of changes in viral parameters.* (a) The higher the initial virus count, the greater is the increase in the rate of formation of chronic infection, but (b) there was no effect on the conditions in the equilibrium phase. (c) Extending the virus lifespan increased the virus count. (d) Increasing the speed of virus movement to 100 grids/tic increased the virus count, but increasing it to 500 grids/tic had the opposite effect, with a slight declining trend. (a) Black bars: number of infections produced; (b–d) black circles: virus count; line: virus count approximation curve; white bars: uninfected cell count; black bars: infected cell count.

established. When the simulation was performed multiple times, the features described above were maintained, and the average values for virus, infected cell, and uninfected cell counts during the equilibrium state were all consistent.

Fig. 1d shows the simulation screen of the RePast. When we attempted setting all the initial parameters to the same values as those in the StarLogo, the results were not consistent. When we recalculated the parameters from the simulation results, in RePast, the parameters were largely maintained at the levels of the settings, but in StarLogo, the lifespans of both cell types became shorter than the settings while the simulation was in progress. We made the results of both simulations consistent by using the same parameters during the actual simulation (Fig. 2a and b).

3.2. Comparison Between Agent-based Simulation Models and Mathematical Simulation Model

We investigated whether the results of a chronic viral infection disease model produced by RePast would be consistent with the results of a mathematical model. For the mathematical model, we carried out an approximate integration using a four-dimensional Runge–Kutta method to ensure that the uninfected cell count and infected cell count would be in the same class. Parameters were always fixed as constant between simulations. The simulation results were consistent for the equilibrium phase, but transitions in virus count during the transient phase varied, with a shift to equilibrium state following two overshoots in the mathematical model, but a monotonic increase following a logistic curve in the agent-based model (Fig. 3). In the mathematical model, when the equilibrium condition was calculated with $dT/dt = dI/dt = dV/dt = 0$, the equilibrium-phase virus count, uninfected cell count, and infected cell count were very similar to those of the agent-based model (virus count: mathematical model 371.8/space, agent-based model 371.1 ± 32.4/space [average ± SD]; uninfected cell count: mathematical model 1605/space, agent-based model 1454 ± 194/space; infected cell count: mathematical model 115.9/space, agent-based model 108.3 ± 14.2/space).

3.3. Usability of the Models; Effect of Changing Parameters

We investigated the changes in the equilibrium phase brought about by changing each parameter. All the investigations below were carried out by using RePast, and we used the average values from ten simulations.

3.4. Viral Parameters

The lower the virus counts at the beginning of the simulation, the lower the probability of a chronic infection (Fig. 4a). However, the initial virus count did not have any effect on the equilibrium

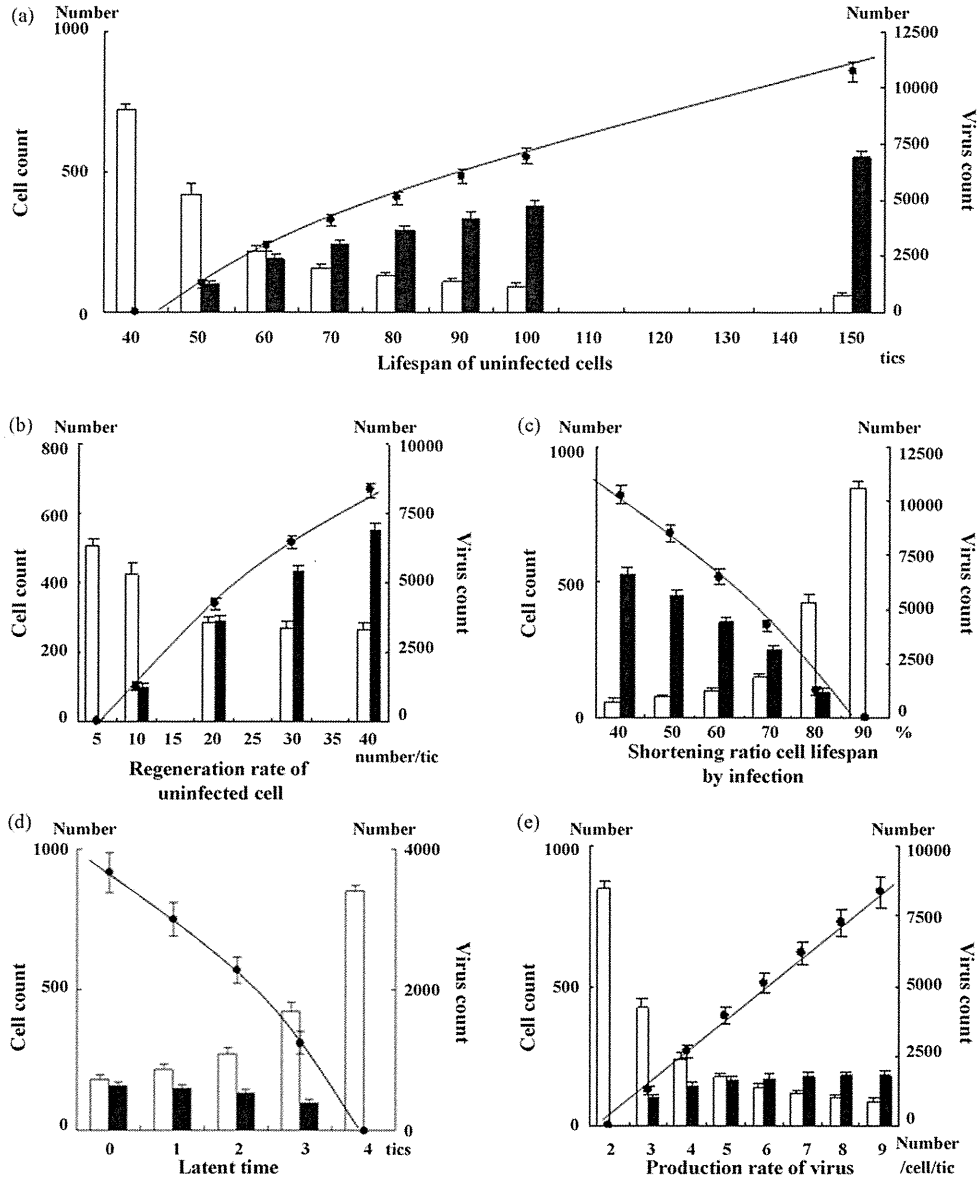

Fig. 5. Effects of changes in cell parameters. (a) Extending the uninfected cell lifespan and (b) increasing the uninfected cell regeneration rate increased the virus count. (c) Raising the lifespan-shortening ratio as a result of infection shortened the lifespan of infected cells, thereby decreasing the virus count. (d) Extending the latent period shortened the period of virus production from infected cells, thereby decreasing the virus count. (e) Increasing the virus production count resulted in a linear increase in equilibrium-phase virus count. Black circles: virus count; line: virus count approximation curve; white bars: uninfected cell count; black bars: infected cell count.

phase itself (Fig. 4b). Extending the lifespan of viruses resulted in a linear increase in equilibrium-phase virus count (Fig. 4c). Although the infected cell count increased, the rate of increase gradually declined. Changing the speed of viral movement resulted in the equilibrium-phase virus count to eventually decline after 100 grids/tic was reached, allowing movement over an area twice the size of the simulation space (Fig. 4d).

3.5. Uninfected Cell Parameters

Extending the lifespan of uninfected cells led to an increased virus count during the equilibrium phase (Fig. 5a). Increasing the uninfected cell regeneration rate also contributed to increased equilibrium-phase virus count (Fig. 5b). In both the cases, the increases in virus count and infected cell count were not linear, but showed a tendency for the rate of increase to decline gradually.

3.6. Infected Cell Parameters

We carried out an investigation of the effects of variation in the lifespan-shortening ratio on the virus count on the assumption that cell lifespan is shortened by infection. When this ratio was increased, the virus count decreased (Fig. 5c). An extended latent period was also related to a decreased virus count (Fig. 5d). However, the virus production from infected cells led to a linear increase in the virus count (Fig. 5e).

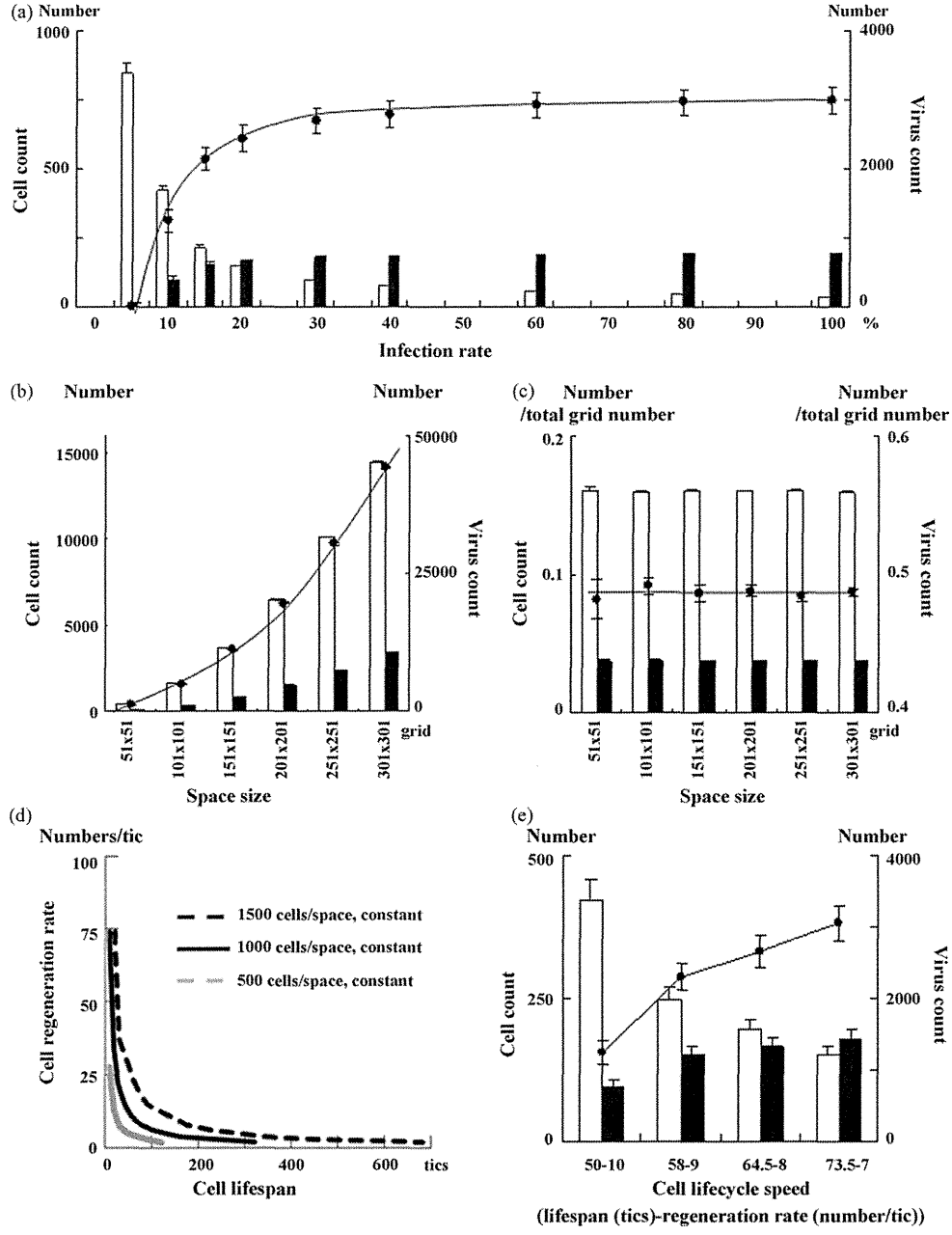

Fig. 6. (a) Increasing the infection rate increased the virus count in equilibrium periods, but the virus count did not change at infection rates of 30% or more. (b) The size of the simulation space increased not only virus count but also the cell count; however, (c) when virus and cell counts were divided by the total number of grids in the space, they were constant for all space sizes. (d) Changing the lifespan and regeneration rate of uninfected cells in opposite directions at the same time makes it possible to change only the cell cycle speed without altering the uninfected cell count. (e) When the cell cycle speed was reduced, the virus count increased toward the right of the graph. This may be because the effect of extending the lifespan of cells exceeds that of reducing their regeneration rate. (a–c and e) Black circles: virus count; line: virus count approximation curve; white bars: uninfected cell count; black bars: infected cell count.

3.7. Infection Rate and Space Size

Increasing the infection rate caused an increase in the virus count, but the change was minimal at an infection rate of 30% or more. The same results were seen for infected cell count, but a decrease in uninfected cell count resulted in a tendency for the infection rate to decrease by up to 60% (Fig. 6a).

The larger the space, higher the increase in both virus and cell counts (Fig. 6b). This increase was proportional to space size, however, when virus and cell counts were divided by the total number of grids in the space they were all constant (Fig. 6c).

3.8. Cell Cycle Speeds

Running a simulation with the initial virus count set to zero enables only the equilibrium condition for uninfected cells to be simulated. Changing the lifespan and regeneration rate of uninfected cells in opposite directions at the same time makes it possible

to change the cell cycle speed without altering the uninfected cell count (Fig. 6d). We used this technique to investigate how changing the cell cycle speed affected the equilibrium phase. Fig. 6e shows the results. Cell lifespan increases while the cell cycle speed declines. The equilibrium virus count increased in accordance with slower cell cycle speeds.

4. Discussion

In this study, we investigated the models using two agent-based simulation methods to program a simple virus–host chronic infection model. The same model written in two different programming language systems displayed the same results. The transient phase was unlike that seen in a mathematical simulation with no overshoot in virus count, but rather a smooth transition to the equilibrium phase. The virus count at the start of the simulation only had effect on the rate of infection development. Increases in virus lifespan, uninfected cell lifespan, uninfected cell regeneration rate, virus production count from infected cells, and infection rate all led to increased equilibrium-phase virus count. Rises in the infected cell lifespan-shortening ratio, latent period, and cell cycle speed decreased the equilibrium-phase virus count. The size of the space itself had no innate effect on the equilibrium phase, but a speed of movement of the virus that was twice the size of the space produced the maximum virus count.

Reproducibility is the basis for all scientific study, but there are many problems to prove it in computer simulations, such as programming bugs. As agent-based simulation deals with numerous agents individually, it requires vast amounts of calculations. Accumulation of very small change of values leads to large differences of results. In this study, we investigated two programs based on two programming languages to confirm the reproducibility of our simulation results in different programming languages. The results of two simulations were consistent, but in StarLogo, the lifespan parameters had a tendency to be lower than when they were set while simulations were actually in progress. This may be because the number of digits used in calculations was different between the two programs. RePast performs calculations to at least eight decimal places. In StarLogo, the library settings only enable settings to be made up to five decimal places. It is probable that these small differences accumulate during repeated calculations and are reflected in the simulation. Ultimately, we confirmed that the differences in results obtained by using different libraries and programming languages were not innate and by making the parameters consistent during simulation, consistent results were obtained.

Mathematical models using formulae for HIV therapy was published in 1994, the method has since been applied to HBV and HCV (Ho et al., 1995; Nowak et al., 1996; Neumann et al., 1998), and they were thought to be good reflections of the reality. In the mathematical model, viruses and cells are conceived as individuals in the concept itself, but both of them are perceived *en masse* when calculations are performed. However a feature of the agent-based simulation is that it deals with individual viruses and cells as separate agents. By moving each agent individually, it probes the factors influencing overall shifts from the micro viewpoint. When the space is viewed as a whole, it is possible to watch on the screen the collective movement of groups of agents. Recently, models that provide a visual representation of Epstein-Barr virus and HIV infection have been reported, both of which are useful for an instinctive and intuitive understanding (Duca et al., 2007; Shapiro et al., 2008; Castiglione et al., 2007).

In agent-based simulation model, virus count transit smoothly to the equilibrium phase. On the other hand, virus counts overshoot during transient phase in mathematical model. We think this difference is derived from technicality of different modeling. The difference in concepts between mathematical models and agent-based models is the space. The mathematical model has no space in concept, but agents move across the space in the agent-based model. In agent-based models, the densities of virus and cells change overtime especially in the transition phase because of the limited space. These changes of the densities of virus and cells lead to the dynamic change of the encounter rate of viruses and cells. The mathematical model does not make such concept of the density; the encounter rate is constant. This may be the reason for the difference between two models in the transition phase. Since no overshoot of virus counts in transient phase had been reported from in vivo studies of hepatitis C virus and simian immunodeficiency virus (Dahari et al., 2005; Nowak et al., 1997), agent-based model correlates with actual biology in vivo at least for these viruses. The increase of initial virus count at the start of simulation correlates with higher encounter rate of viruses and cells which make the linear increasing of infection forming rate. Mathematical model can only express the infection formation rate as "infected or not".

The importance of viral passing speed in the agent-based model is also explained by the "space". Although the virus actually moves through the blood stream in our body and virus could not decide their moving speeds by themselves, there is most appropriate speed for virus to meet the cells on the simulation space by the highest probability. The effect of cell cycle speed should be mentioned by another affection of the space. A fast cell cycle speed means that the lifespan of uninfected cells is short. Then fast cell cycle speed leads to the short lifespan of infected cells. A higher regeneration rate for uninfected cells results in a higher rate of infection among uninfected cells by viruses, but in situations where viruses and cells are dispersed around the space this is ineffective in increasing the infection rate, as the latter depends on the probability that they will encounter one another. As a result, the infected cell count decreases during the equilibrium phase, as does the virus count.

In this study, we confirmed the reproducibility and usability of agent-based models in expressing the interaction between viruses and cells. A feature of this simulation system is that it uses the concept of space as actual space, which means that the existence of the space becomes an additional controlling factor on the simulation results. This is a concept that is absent from mathematical models. The reality is that we have a spatial existence, and an advantage of the agent-based simulation system is the fact that it accounts for the space. Another feature of the simulation system is that it enables the condition to be perceived in visual terms, making it easy to understand. However it may be affected by computer performance and by the limitations of programming languages or the program itself, this system may offer a powerful tool for the future analysis of real virus–host interaction disease.

Conflict of interest

No conflicts of interest exist for all authors.

References

Castiglione, F., Pappalardo, F., Bernaschi, M., Motta, S., 2007. Optimization of HAART with genetic algorithms and agent-based models of HIV infection. Bioinformatics 23, 3350–3355, doi:10.1093/bioinformatics/btm408.

Dahari, H., Major, M., Zhang, X., Mihalik, K., Rice, C.M., Perelson, A.S., Feinstone, S.M., Neumann, A.U., 2005. Mathematical modeling of primary hepatitis c infection: noncytolytic clearance and early blockage of virion production. Gastroenterology 128, 1056–1066, doi:10.1053/j.gastro.2005.01.049.

Duca, K.A., Shapiro, M., Delgado-Eckert, E., Hadinoto, V., Jarrah, A.S., Laubenbacher, R., Lee, K., Luzuriaga, K., Polys, N.F., Thorley-Lawson, D.A., 2007. A virtual look at Epstein-Barr virus infection: biological interpretations. PLoS Pathog. 3, 1388–1400, doi:10.1371/journal.ppat.0030137.

Gilbert, N., Bankes, S., 2002. Platforms and methods for agent-based modelling. Proc. Natl. Acad. Sci. U.S.A. 99 (Suppl. 3), 7197–7198.

Ho, D.D., Neumann, A.U., Perelson, A.S., Chen, W., Leonard, J.M., Markowitz, M., 1995. Rapid turnover of plasma virions and CD4 lymphocytes in HIV-1 infection. Nature 373, 123–126, doi:10.1038/373123a0.

Naniche, D., 2009. Human immunology of measles virus infection. Curr. Top. Microbiol. Immunol. 330, 151–171.

Neumann, A.U., Lam, N.P., Dahari, H., Gretch, D.R., Wiley, T.E., Layden, T.J., Perelson, A.S., 1998. Hepatitis C viral dynamics in vivo and the antiviral efficacy of interferon-alpha therapy. Science 282, 103–107, doi:10.1126/science.282.5386.103.

Nowak, M.A., Bonhoeffer, S., Hill, A.M., Boehme, R., Thomas, H.C., McDade, H., 1996. Viral dynamics in hepatitis B virus infection. Proc. Natl. Acad. Sci. U.S.A. 93, 4398–4402.

Nowak, M.A., Lloyd, A.L., Vasquez, G.M., Wiltrout, T.A., Wahl, L.M., Biscofberger, N., Williams, J., Kinter, A., Fauci, A.S., Hirsch, V.M., Lifson, J.D., 1997. Viral dynamics of primary viremia and antiretroviral therapy in simian immunodeficiency virus infection. J. Virol. 71, 7518–7525.

Shapiro, M., Duca, K.A., Lee, K., Delgado-Eckert, E., Hawkins, J., Jarrah, A.S., Laubenbacher, R., Polys, N.F., Hadinoto, V., Thorley-Lawson, D.A., 2008. A virtual look at Epstein-Barr virus infection: simulation mechanism. J. Theor. Biol. 252, 633–648, doi:10.1016/j.jtbi.2008.01.032.

See, H., Wark, P., 2008. Innate immune response to viral infection of the lungs. Paediatr. Respir. Rev. 9, 243–250, doi:10.1016/j.prrv.2008.04.001.

OPEN ACCESS

ORIGINAL ARTICLE

Hepatitis C virus kinetics by administration of pegylated interferon-α in human and chimeric mice carrying human hepatocytes with variants of the *IL28B* gene

Tsunamasa Watanabe,[1] Fuminaka Sugauchi,[2] Yasuhito Tanaka,[1] Kentaro Matsuura,[3] Hiroshi Yatsuhashi,[4] Shuko Murakami,[1] Sayuki Iijima,[1] Etsuko Iio,[3] Masaya Sugiyama,[5] Takashi Shimada,[6] Masakazu Kakuni,[6] Michinori Kohara,[7] Masashi Mizokami[5]

► Additional supplementary files are published online only. To view these files please visit the journal online (http://dx.doi.org/10.1136/gutjnl-2012-302553).

[1]Department of Virology and Liver Unit, Nagoya City University Graduate School of Medical Sciences, Nagoya, Japan
[2]Department of Gastroenterology, Nagoya City Koseiin Medical Welfare Center, Nagoya, Japan
[3]Department of Gastroenterology and Metabolism, Nagoya City University Graduate School of Medical Sciences, Nagoya, Japan
[4]Department of Therapeutic Research, National Hospital Organization (NHO) Nagasaki Medical Center, Nagasaki, Japan
[5]The Research Center for Hepatitis and Immunology, National Center for Global Health and Medicine, Ichikawa, Japan
[6]PhoenixBio Co. Ltd., Higashi-Hiroshima, Japan
[7]Tokyo Metropolitan Institute of Medical Science, Tokyo, Japan

Correspondence to
Dr Masashi Mizokami, The Research Center for Hepatitis and Immunology, National Center for Global Health and Medicine 1–7–1, Kohnodai, Ichikawa 272–8516, Japan; mmizokami@hospk.ncgm.go.jp

Revised 4 October 2012
Accepted 9 October 2012

ABSTRACT

Objective Recent studies have demonstrated that genetic polymorphisms near the *IL28B* gene are associated with the clinical outcome of pegylated interferon α (peg-IFN-α) plus ribavirin therapy for patients with chronic hepatitis C virus (HCV). However, it is unclear whether genetic variations near the *IL28B* gene influence hepatic interferon (IFN)-stimulated gene (ISG) induction or cellular immune responses, lead to the viral reduction during IFN treatment.

Design Changes in HCV-RNA levels before therapy, at day 1 and weeks 1, 2, 4, 8 and 12 after administering peg-IFN-α plus ribavirin were measured in 54 patients infected with HCV genotype 1. Furthermore, we prepared four lines of chimeric mice having four different lots of human hepatocytes containing various single nucleotide polymorphisms (SNP) around the *IL28B* gene. HCV infecting chimeric mice were subcutaneously administered with peg-IFN-α for 2 weeks.

Results There were significant differences in the reduction of HCV-RNA levels after peg-IFN-α plus ribavirin therapy based on the *IL28B* SNP rs8099917 between TT (favourable) and TG/GG (unfavourable) genotypes in patients; the first-phase viral decline slope per day and second-phase slope per week in TT genotype were significantly higher than in TG/GG genotype. On peg-IFN-α administration to chimeric mice, however, no significant difference in the median reduction of HCV-RNA levels and the induction of antiviral ISG was observed between favourable and unfavourable human hepatocyte genotypes.

Conclusions As chimeric mice have the characteristic of immunodeficiency, the response to peg-IFN-α associated with the variation in *IL28B* alleles in chronic HCV patients would be composed of the intact immune system.

Significance of this study

What is already known on this subject?

- Genetic polymorphisms near the *IL28B* gene are associated with a chronic HCV treatment response.
- HCV-infected patients with the *IL28B* homozygous favourable allele had a more rapid decline in HCV kinetics in the first and second phases by peg-IFN-α-based therapy.
- During the acute phase of HCV infection, a strong immune response among patients with the *IL28B* favourable genotype could induce more frequent spontaneous clearance of HCV.

What are the new findings?

- In chronically HCV genotype 1b-infected chimeric mice that have the characteristic of immunodeficiency, no significant difference in the reduction in serum HCV-RNA levels and the induction of antiviral hepatic ISG by the administration of peg-IFN-α was observed between favourable and unfavourable human hepatocyte *IL28B* genotypes.
- By comparison of serum HCV kinetics between human and chimeric mice, the viral decline in both the first and second phases by peg-IFN-α treatment was affected by the variation in *IL28B* genotypes only in chronic hepatitis C patients.

How might it impact on clinical practice in the foreseeable future?

- The immune response according to *IL28B* genetic variants could contribute to the first and second phases of HCV-RNA decline and might be critical for HCV clearance by peg-IFN-α-based therapy.

INTRODUCTION

Hepatitis C is a global health problem that affects a significant portion of the world's population. The WHO estimated that, in 1999, 170 million hepatitis C virus (HCV)-infected patients were present worldwide, with 3–4 million new cases appearing per year.[1]

The standard therapy for hepatitis C still consists of pegylated interferon-α (peg-IFN-α), administered once weekly, plus daily oral ribavirin for 24–48 weeks in countries where protease inhibitors are not available.[2] This combination therapy is quite successful in patients with HCV genotype 2 or 3 infection, leading to a sustained virological response (SVR) in approximately 80–90% of patients treated; however, in patients infected with HCV genotype 1 or 4, only approximately half of all treated individuals achieved a SVR.[3 4]

Table 1 Characteristics of 54 patients infected HCV genotype 1

	IL28B SNP rs8099917		
	TT (n=34)	TG (n=19) + GG (n=1)	p Value
Age (years)	55.6±10.1	54.7±11.3	0.746
Gender (male %)	70	50	0.199
Body mass index (kg/m^2)	24.6±3.1	24.7±3.3	0.870
Viral load at therapy (log IU/ml)	6.0±0.7	5.8±0.8	0.357
SVR rate (%)	50	11	0.012
Serum ALT level (IU/l)	100.3±80.8	79.3±45.0	0.226
Platelet count (×10^4/μl)	17.1±9.0	16.5±5.8	0.771
Fibrosis (F3+4 %)	42	40	0.877

HCV, hepatitis C virus; SNP, single nucleotide polymorphism; SVR, sustained virological response.

Host factors were shown to be associated with the outcome of the therapy, including age, sex, race, liver fibrosis and obesity.[5] Genome-wide association studies have demonstrated that genetic variations in the region near the interleukin-28B (*IL28B*) gene, which encodes interferon (IFN)-λ3, are associated with a chronic HCV treatment response.[6–10] Furthermore, it was demonstrated that genetic variations in the *IL28B* gene region are also associated with spontaneous HCV clearance.[11–12]

Interestingly, a recent report showed the effect of genetic polymorphisms near the *IL28B* gene on the dynamics of HCV during peg-IFN-α plus ribavirin therapy in Caucasian, African American and Hispanic individuals;[13] HCV-infected patients with the *IL28B* homozygous favourable allele had a more rapid decline of HCV in the first phase, which is associated with the inhibition of viral replication as well as the second phase associated with immuno-destruction of viral-infected hepatocytes.[14] However, it is unknown how a direct effect by the *IL28B* genetic variation, such as the induction of IFN-stimulated genes (ISG) or cellular immune responses, would influence the viral kinetics during IFN treatment. Over recent periods, engineered severe combined immunodeficient (SCID) mice transgenic for urokinase-type plasminogen activator (uPA) received human hepatocyte transplants (hereafter referred to as chimeric mice)[15–17] and are suitable for experiments with hepatitis viruses in vivo.[18 19] We have also reported that these chimeric mice carrying human hepatocytes are a robust animal model to evaluate the efficacy of IFN and other anti-HCV agents.[20 21]

The purpose of this study was to reveal the association between genetic variations in the *IL28B* gene region and viral decline during peg-IFN-α treatment in patients with HCV, and to clarify the association between different *IL28B* alleles of human hepatocytes in chimeric mice and the response to peg-IFN-α without immune response. These studies will elucidate whether the immune response by the *IL28B* genetic variation affects the viral kinetics during peg-IFN-α treatment.

MATERIALS AND METHODS

Patients

Fifty-four Japanese patients with chronic HCV genotype 1 infection at Nagasaki Medical Center and Nagoya City University were enrolled in this study (table 1). Patients received peg-IFN-α2a (180 μg) or 2b (1.5 μg/kg) subcutaneously every week and were administered a weight-adjusted dose of ribavirin (600 mg for <60 kg, 800 mg for 60–80 kg, and 1000 mg for >80 kg daily), which is the recommended dosage in Japan. Patients with other hepatitis virus infection or HIV coinfection were not included in the study. The study protocol conformed to the ethics guidelines of the 1975 Declaration of Helsinki as reflected by earlier approval by the institutions' human research committees.

Laboratory tests

Blood samples were obtained before therapy, as well as on day 1 and at weeks 1, 2, 4, 8 and 12 after the start of therapy and were analysed for the HCV-RNA level by the commercial Abbott Real-Time HCV test with a lower limit of detection of 12 IU/ml (Abbott Molecular Inc., Des Plains, Illinois, USA). Genetic polymorphism in the *IL28B* gene (rs8099917), a single nucleotide polymorphism (SNP) recently identified to be associated with treatment response,[6–8] was tested by the TaqMan SNP genotyping assay (Applied Biosystems, Foster City, California, USA).

HCV infection of chimeric mice with the liver repopulated for human hepatocytes

SCID mice carrying the uPA transgene controlled by an albumin promoter were injected with 5.0–7.5×10^5 viable hepatocytes through a small left-flank incision into the inferior splenic pole, thereafter chimeric mice were generated. The chimeric mice were purchased from PhoenixBio Co, Ltd (Hiroshima, Japan).[17] Human hepatocytes with the *IL28B* homozygous favourable allele, heterozygous allele or homozygous unfavourable allele were imported from BD Biosciences (San Jose, California, USA) (table 2). Murine serum levels of human albumin and the body weight were not significantly different among four chimeric mice groups, providing a reliable comparison for anti-HCV agents.[22] Three different serum samples were obtained from three chronic HCV patients (genotype 1b).[21 22] Each mouse was intravenously infected with serum sample containing 10^5 copies of HCV genotype 1b. Administration of peg-IFN-α2a (Pegasys; Chugai Pharmaceutical Co., Ltd., Tokyo, Japan) at the dose formulation (30 μg/kg) was consecutively applied to each mouse on days 0, 3, 7 and 10 (table 3).

HCV-RNA quantification

HCV-RNA in mice sera (days 0, 1, 3, 7 and 14) was quantified by an in-house real-time detection PCR assay with a lower quantitative limit of detection of 10 copies/assay, as previously reported.[21]

Quantification of IFN-stimulated gene-expression levels

For analysis of endogenous ISG levels, total RNA was isolated from the liver using the RNeasy RNA extraction kit (Qiagen, Valencia, California, USA) and complementary DNA synthesis

Table 2 Four lines of uPA/SCID mice from four different lots of human hepatocytes (donor) containing various SNP around the *IL28B* gene

uPA/SCID mice	Donor	Race	Age	Gender	rs8103142	rs12979860	rs8099917
PXB mice	A	African American	5 Years	Male	CC	TT	TG
	B	Caucasian	10 Years	Female	CC	TT	TG
	C	Hispanic	2 Years	Female	TT	CC	TT
	D	Caucasian	2 Years	Male	TT	CC	TT

PXB mice; urokinase-type plasminogen activator/severe combined immunodeficiency (uPA/SCID) mice repopulated with approximately 80% human hepatocytes.
SCID, severe combined immunodeficient; SNP, single nucleotide polymorphism.

Table 3 Dosage and time schedule of pegIFN-α2a* treatment for HCV genotype 1b infected chimeric mice

Donor hepatocytes†	No of chimeric mice	Inoculum	Test compound	Dose			
				Level (μg/kg)	Concentrtion (μg/ml)	Volume (ml/kg)	Frequency
A	3	Serum A	Peg-IFN-α2a	30	3	10	Day 0, 3, 7, 10
B	4	Serum A	Peg-IFN-α2a	30	3	10	Day 0, 3, 7, 10
C	3	Serum A	Peg-IFN-α2a	30	3	10	Day 0, 3, 7, 10
D	3	Serum A	Peg-IFN-α2a	30	3	10	Day 0, 3, 7, 10
A	2	Serum B	Peg-IFN-α2a	30	3	10	Day 0, 3, 7, 10
C	2	Serum B	Peg-IFN-α2a	30	3	10	Day 0, 3, 7, 10
A	2	Serum C	Peg-IFN-α2a	30	3	10	Day 0, 3, 7, 10
C	2	Serum C	Peg-IFN-α2a	30	3	10	Day 0, 3, 7, 10

*Pegasys; Chugai Pharmaceutical Co., Ltd., Tokyo, Japan.
†The *IL28B* genetic variation of the donor hepatocytes was indicated in table 2.
HCV, hepatitis C virus; peg-IFN-α, pegylated interferon α.

was performed using 2.0 μg of total RNA (High Capacity RNA-to-cDNA kit; Applied Biosystems). Fluorescence real-time PCR analysis was performed using an ABI 7500 instrument (Applied Biosystems) and TaqMan Fast Advanced gene expression assay (Applied Biosystems). TaqMan Gene Expression Assay primer and probe sets (Applied Biosystems) are shown in the supplementary information (available online only). Relative amounts of messenger RNA, determined using a FAM-Labeled TaqMan probe, were normalised to the endogenous RNA levels of the housekeeping reference gene, glyceraldehyde-3-phosphate dehydrogenase. The delta Ct method ($2^{-(\text{delta Ct})}$) was used for quantitation of relative mRNA levels and fold induction.[23 24]

Statistical analyses

Statistical differences were evaluated by Fisher's exact test or the χ^2 test with the Yates correction. Mice serum HCV-RNA and intrahepatic ISG expression levels were compared using the Mann–Whitney U test. Differences were considered significant if p values were less than 0.05.

RESULTS

Characteristics of the study patients

Genotypes (rs8099917) TT, TG and GG were detected in 34, 19 and one patient infected with HCV genotype 1, respectively. SVR rates were significantly higher in HCV patients with genotype TT than in those with genotype TG/GG (50% vs 11%, p=0.012). The initial HCV serum load was comparable between genotypes TT and TG/GG (6.0±0.7 vs 5.8±0.8 log IU/ml). There were no significant differences in sex (male%, 70% vs 50%), age (55.6±10.1 vs 54.7±11.3 years), serum alanine aminotransferase level (100.3±80.8 vs 79.3±45.0 IU/L), platelet count (17.1±9.0 vs 16.5±5.8×10^4/μl) and fibrosis stages (F3/4%, 42% vs 40%) between HCV patients with the favourable (rs8099917 TT) and unfavourable (rs8099917 TG/GG) *IL28B* genotypes (table 1).

Changes in serum HCV-RNA levels in patients treated by peg-IFN-α plus ribavirin

Figure 1 shows the initial change in the serum HCV-RNA level for 14 days after peg-IFN-α plus ribavirin therapy in patients infected with HCV genotype 1 based on the genetic polymorphism near the *IL28B* gene. The immediate antiviral response (viral drop 24 h after the first IFN injection) was significantly higher in HCV patients with genotype TT than genotype TG/GG (−1.08 vs −0.39 log IU/ml, p<0.001). Figure 2 also shows the subsequent change in the serum HCV-RNA reduction after peg-IFN-α plus ribavirin therapy in patients infected with HCV genotype 1. Similarly, during peg-IFN-α plus ribavirin therapy, a statistically significant difference in the median reduction in serum HCV-RNA levels was noted according to the genotype (TT vs TG/GG). The median reduction in the serum HCV-RNA levels (log IU/ml) at 1, 2, 4, 8 and 12 weeks between genotypes TT and TG/GG was as follows: −1.58 vs −0.62, p<0.001; −2.35 vs −0.91, p<0.001;

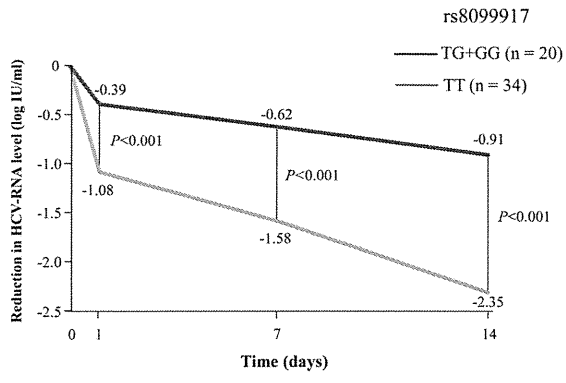

Figure 1 Rapid reduction of median hepatitis C virus (HCV)-RNA levels (log IU/ml) at 1, 7 and 14 days between *IL28B* single nucleotide polymorphisms rs8099917 genotype TT (n=34) and TG/GG (n=20) in HCV genotype 1-infected patients treated with peg-IFN-α plus ribavirin.

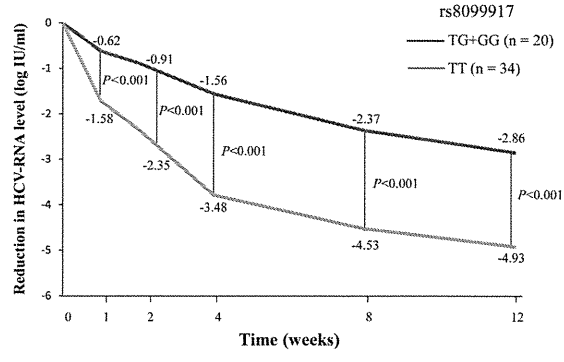

Figure 2 Weekly reduction of median hepatitis C virus (HCV)-RNA levels (log IU/ml) at 1, 2, 4, 8 and 12 weeks between *IL28B* single nucleotide polymorphisms rs8099917 genotype TT (n=34) and TG/GG (n=20) in HCV genotype 1-infected patients treated with pegylated interferon α plus ribavirin.

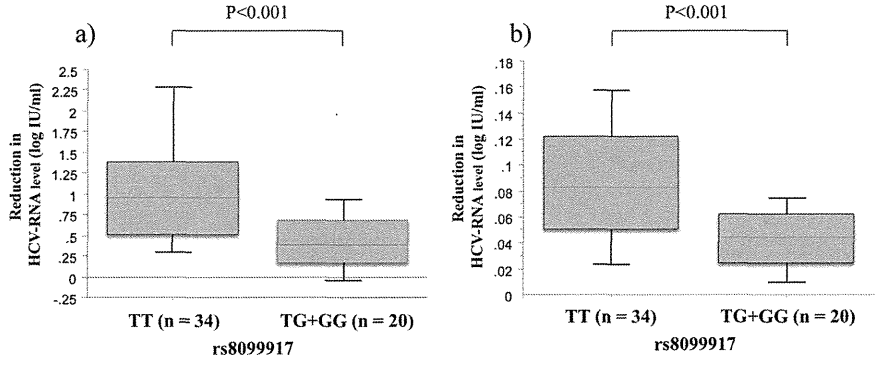

Figure 3 (A) The first-phase viral decline slope per day (Ph1/day) and (B) second-phase viral decline slope per week (Ph2/week) in hepatitis C virus (HCV) genotype 1-infected patients treated with pegylated interferon α plus ribavirin. The lines across the boxes indicate the median values. The hash marks above and below the boxes indicate the 90th and 10th percentiles for each group, respectively.

−3.48 vs −1.56, p<0.001; −4.53 vs −2.37, p<0.01; −4.93 vs −2.86, p<0.001. Furthermore, the initial first-phase viral decline slope per day (Ph1/day) and subsequent second-phase viral decline slope per week (Ph2/week) in TT genotype were significantly higher than in genotype TG/GG (Ph1/day 0.94 ±0.83 vs 0.38±0.40 log IU/ml, p<0.001; Ph2/week 0.08±0.06 vs 0.04±0.03 log IU/ml, p<0.001) (figure 3).

Changes in serum HCV-RNA levels in chimeric mice treated by peg-IFN-α

In order to clarify the association between *IL28B* alleles of human hepatocytes and the response to peg-IFN-α, we prepared four lines of uPA/SCID mice and four different lots of human hepatocytes containing various rs8099917, rs8103142 and rs12979860 SNPs around the *IL28B* gene (table 2). The chimeric mice were inoculated with serum samples from each HCV-1b patient, and then HCV-RNA levels had increased and reached more than 10^6 copies/ml in all chimeric mice sera at 2 weeks after inoculation. After confirming the peak of HCV-RNA in all chimeric mice, they were subcutaneously administered with four times injections of the bolus dose of peg-IFN-α2a for 2 weeks (table 3). Figure 4 shows the change in the serum HCV-RNA levels for 14 days during IFN injection into chimeric mice transplanted with *IL28B* favourable or unfavourable human hepatocyte genotypes. On peg-IFN-α administration, no significant difference in the median reduction in HCV-RNA levels in the serum A-infected[22] chimeric mice sera was observed between favourable (n=7) and unfavourable

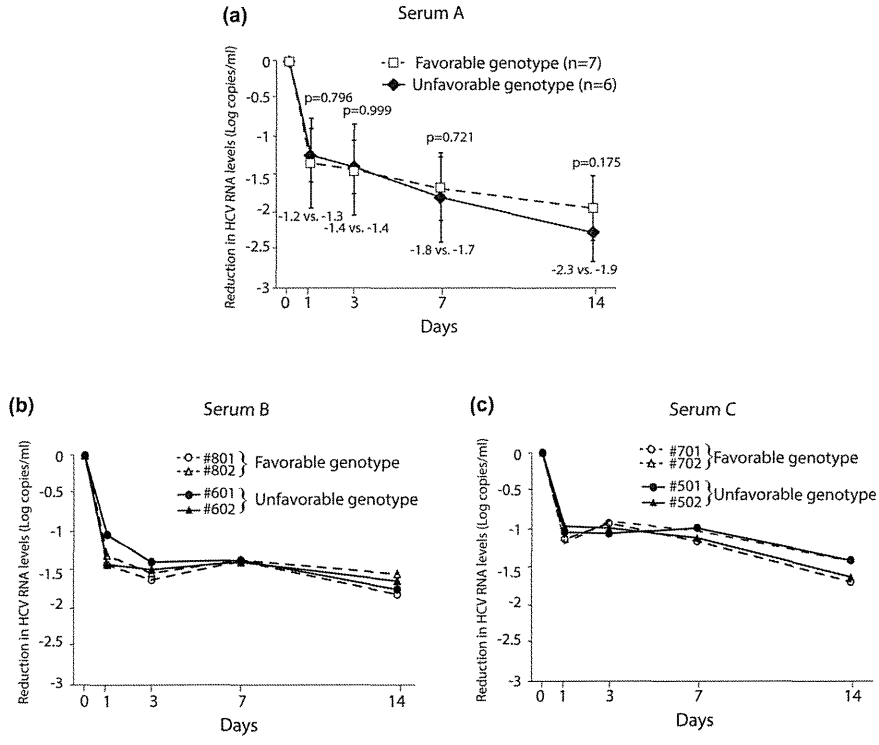

Figure 4 Median reduction of hepatitis C virus (HCV)-RNA levels (log copies/ml) after administering pegylated interferon α to chimeric mice having human hepatocytes containing various single nucleotide polymorphisms around the *IL28B* gene as favourable (rs8099917 TT) and unfavourable (rs8099917 TG) genotypes. Data are represented as mean+SD. Chimeric mice infected with a) serum A (n=7; favourable genotype, n=6; unfavourable genotype), (B) serum B (n=2, each genotype), and (C) serum C (n=2, each genotype). All serum samples were obtained from HCV-1b patients.

(n=6) *IL28B* genotypes on days 1, 3, 7 and 14 (−1.2 vs −1.3, −1.4 vs −1.4, −1.8 vs −1.7, and −2.3 vs −1.9 log copies/ml) (figure 4A). Moreover, we prepared two additional serum samples from the other HCV-1b patients (serum B and C)[21] to confirm the influence of *IL28B* genotype in early viral kinetics during IFN treatment. After establishing persistent infection with new HCV-1b strains in all chimeric mice, they were also administered four times injections of the bolus dose of peg-IFN-α2a for 2 weeks (figure 4B,C). In a similar fashion, no significant difference in HCV-RNA reduction in chimeric mice sera was observed between favourable and unfavourable *IL28B* genotypes.

Expression levels of ISG in chimeric mice livers

Because chimeric mice have the characteristic of severe combined immunodeficiency, the viral kinetics in chimeric mice sera during IFN treatment could be contributed by the innate immune response of HCV-infected human hepatocytes. Therefore, ISG expression levels in mice livers transplanted with human hepatocytes were compared between favourable and unfavourable *IL28B* genotypes (figure 5).

As shown in figure 5A, ISG expression levels in mice livers were measured at 8 h and 24 h after IFN treatment. The levels of representative antiviral ISG (eg, myxovirus resistance protein A, oligoadenylate synthetase 1, RNA-dependent protein kinase) and other ISG for promoting antiviral signalling (eg, Toll-like receptor 3, retinoic acid-inducible gene 1) were significantly induced at least 8 h after treatment, and prolonged at 24 h. No significant difference in ISG expression levels in HCV-infected livers was observed between favourable and unfavourable *IL28B* genotypes. The other inoculum for persistent infection of HCV-1b also demonstrated no significant difference in ISG

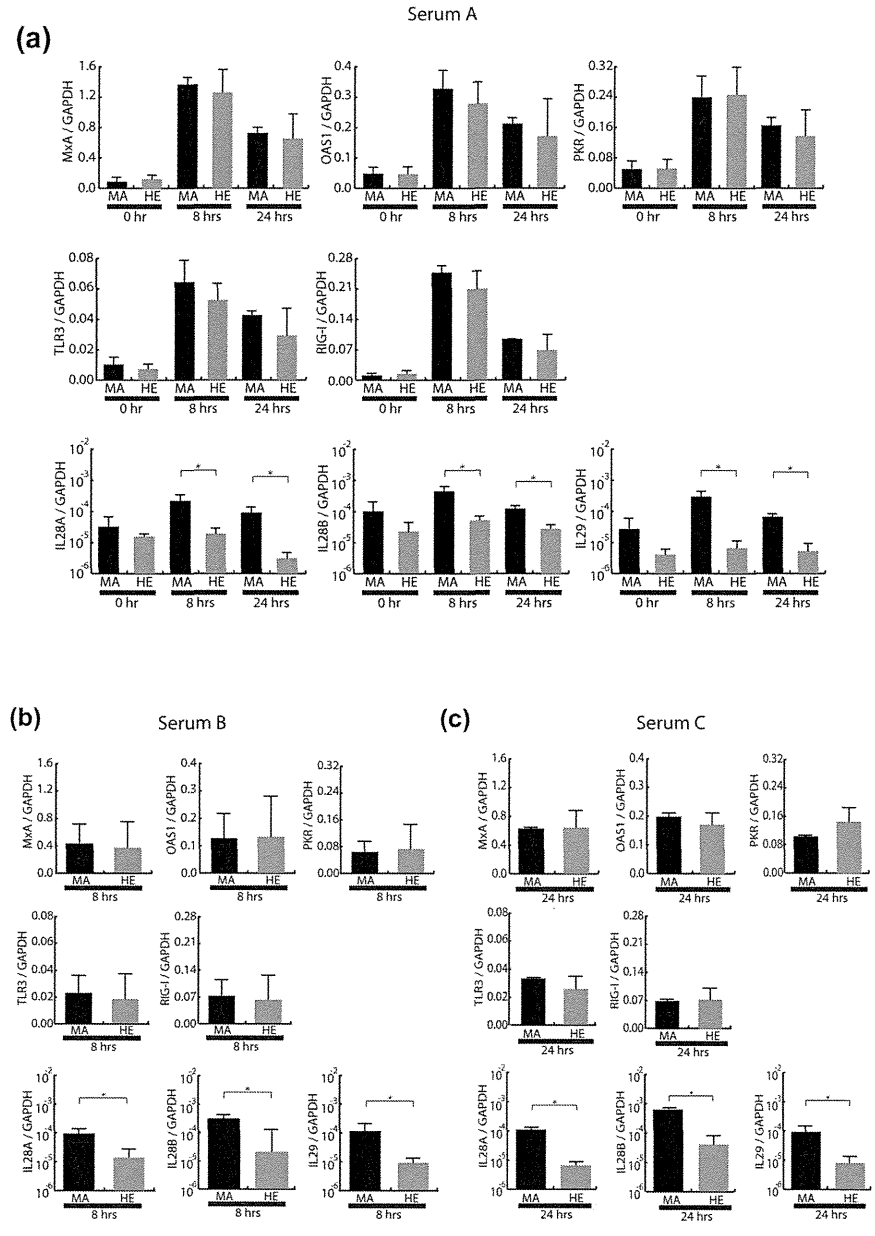

Figure 5 Intrahepatic interferon (IFN)-stimulated gene (ISG) expression levels in the pegylated interferon α (peg-IFN-α)-treated chimeric mice having human hepatocytes containing homozygous favourable allele (rs8099917 TT; MA) and heterozygous unfavourable allele (rs8099917 TG; HE) were measured and expressed relative to glyceraldehyde-3-phosphate dehydrogenase (GAPDH) messenger RNA. Data are represented as mean+SD. (A) Time kinetics of ISG after administration of the peg-IFN-α in serum A-infected chimeric mice (n=3, each genotype). Comparison of ISG expression levels at (B) 8 h in serum B-infected mice and (C) 24 h in serum C-infected mice after administering peg-IFN-α (n=3, each genotype). Predesigned real-time PCR assay of IL28B transcript purchased from Applied Biosystems can be cross-reactive to IL28A transcript. *p<0.05. MxA, myxovirus resistance protein A; OAS1, oligoadenylate synthetase 1; PKR, RNA-dependent protein kinase; RIG-1, retinoic acid-inducible gene 1; TLR3, Toll-like receptor 3.

expression levels between favourable and unfavourable *IL28B* genotypes (figure 5B,C). Interestingly, IFN-λ expression levels by treatment of peg-IFN-α were significantly induced in HCV-infected human hepatocytes harbouring the favourable *IL28B* genotype (figure 5 A–C).

DISCUSSION

Several recent studies have demonstrated a marked association between the chronic hepatitis C treatment response[6–9] and SNP (rs8099917, rs8103142 and rs12979860) near or within the region of the *IL28B* gene, which affected the viral dynamics during peg-IFN-α plus ribavirin therapy in Caucasian, African American and Hispanic individuals.[13]

It has been reported that when patients with chronic hepatitis C are treated by IFN-α or peg-IFN-α plus ribavirin, HCV-RNA generally declines after a 7–10 h delay.[25] The typical decline is biphasic and consists of a rapid first phase lasting for approximately 1–2 days during which HCV-RNA may fall 1–2 logs in patients infected with genotype 1, and subsequently a slower second phase of HCV-RNA decline.[26] The viral kinetics had a predictive value in evaluating antiviral efficacy.[14] In this study, biphasic decline of the HCV-RNA level during peg-IFN-α treatment was observed in both patients and chimeric mice infected with HCV genotype 1; however, in the first and second phases of viral kinetics, a difference between *IL28B* genotypes was observed only in HCV-infected patients; a more rapid decline in serum HCV-RNA levels after administering peg-IFN-α plus ribavirin was confirmed in patients with the TT genotype of rs8099917 compared to those with the TG/GG genotype.

On the other hand, in-vivo data using the chimeric mouse model showed no significant difference in the reduction of HCV-RNA titers in mouse serum among four different lots of human hepatocytes containing *IL28B* favourable (rs8099917 TT) or unfavourable (rs8099917 TG) genotypes, which was confirmed by the inoculation of two additional HCV strains. These results indicated that variants of the *IL28B* gene in donor hepatocytes had no influence on the response to peg-IFN-α under immunosuppressive conditions, suggesting that the immune response according to *IL28B* genetic variants could contribute to the first and second phases of HCV-RNA decline and might be critical for HCV clearance by peg-IFN-α-based therapy.

Two recent studies indeed revealed an association between the *IL28B* genotype and the expression level of hepatic ISG in human studies.[27 28] Quiescent hepatic ISG before treatment among patients with the *IL28B* favourable genotype have been associated with sensitivity to exogenous IFN treatment and viral eradication; however, it is difficult to establish whether the hepatic ISG expression level contributes to viral clearance independently or appears as a direct consequence of the *IL28B* genotype. Another recent study addressed this question and the results suggested that there is no absolute correlation with the *IL28B* genotype and hepatic expression of ISG.[29] Our results on the hepatic ISG expression level in immunodeficient chimeric mice also suggested that no significant difference in ISG expression levels was observed between favourable and unfavourable *IL28B* genotypes. However, these results were not consistent with a previous report using chimeric mice that the favourable *IL28B* genotype was associated with an early reduction in HCV-RNA by ISG induction.[30] The reasons for the discrepancy might depend on the dose and type of IFN treatment, as well as the time point when ISG expression was examined in the liver. In addition, although IFN-λ transcript levels measured in peripheral blood mononuclear cells or liver revealed inconsistent results in the context of an association with the *IL28B* genotype,[7 8] our preliminary assay on the IL28A, IL28B and IL29 transcripts in the liver first indicated that the induction of IFN-λ on peg-IFN-α administration could be associated with the *IL28B* genotype. Therefore, the induction of IFN-λ followed by immune response might contribute to different viral kinetics and treatment outcomes in HCV-infected patients, because no difference was found in chimeric mice without immune response.

It has also been reported that the mechanism of the association of genetic variations in the *IL28B* gene and spontaneous clearance of HCV may be related to the host innate immune response.[11] Interestingly, participants with seroconversion illness with jaundice were more frequently rs8099917 homozygous favourable allele (TT) than other genotypes (32% vs 5%, p=0.047). This suggests that a stronger immune response during the acute phase of HCV infection among patients with the *IL28B* favourable genotype would induce more frequent spontaneous clearance of HCV.

Taking into account both the above results in acute HCV infection and our results conducted on chimeric mice that have the characteristic of immunodeficiency, it is suggested that the response to peg-IFN-α associated with the variation in *IL28B* alleles in chronic hepatitis C patients would be composed of the intact immune system.

Acknowledgements The authors would like to thank Kyoko Ito of Nagoya City University Graduate School of Medical Sciences, Nagoya, Japan for doing the quantification of gene-expression assays.

Contributors YT and MM conceived the study. TW and FS and YT conducted the study equally. TW and FS coordinated the analysis and manuscript preparation. All the authors had input into the study design, patient recruitment and management or mouse management and critical revision of the manuscript for intellectual content. TW, FS and YT contributed equally.

Funding This study was supported by a grant-in-aid from the Ministry of Health, Labour, and Welfare of Japan (H22-kannen-005) and the Ministry of Education, Culture, Sports, Science and Technology, Japan, and grant-in-aid for research in Nagoya City University.

Competing interests None.

Patient consent Obtained.

Ethics approval This study was conducted with the approval of each ethics committee at the Nagoya City University and Nagasaki Medical Center (see supplementary information, available online only).

Provenance and peer review Not commissioned; externally peer reviewed.

REFERENCES

1. **Ray Kim W.** Global epidemiology and burden of hepatitis C. *Microbes Infect* 2002;**4**:1219–25.
2. **Foster GR.** Past, present, and future hepatitis C treatments. *Semin Liver Dis* 2004;**24**(Suppl. 2):97–104.
3. **Fried MW,** Shiffman ML, Reddy KR, *et al*. Peginterferon alfa-2a plus ribavirin for chronic hepatitis C virus infection. *N Engl J Med* 2002;**347**:975–82.
4. **Manns MP,** McHutchison JG, Gordon SC, *et al*. Peginterferon alfa-2b plus ribavirin compared with interferon alfa-2b plus ribavirin for initial treatment of chronic hepatitis C: a randomised trial. *Lancet* 2001;**358**:958–65.
5. **Mihm U,** Herrmann E, Sarrazin C, *et al*. Review article: predicting response in hepatitis C virus therapy. *Aliment Pharmacol Ther* 2006;**23**:1043–54.
6. **Ge D,** Fellay J, Thompson AJ, *et al*. Genetic variation in IL28B predicts hepatitis C treatment-induced viral clearance. *Nature* 2009;**461**:399–401.
7. **Suppiah V,** Moldovan M, Ahlenstiel G, *et al*. IL28B is associated with response to chronic hepatitis C interferon-alpha and ribavirin therapy. *Nat Genet* 2009;**41**:1100–4.
8. **Tanaka Y,** Nishida N, Sugiyama M,, *et al* Genome-wide association of IL28B with response to pegylated interferon-alpha and ribavirin therapy for chronic hepatitis C. *Nat Genet* 2009;**41**:1105–9.
9. **Rauch A,** Kutalik Z, Descombes P, *et al*. Genetic variation in IL28B is associated with chronic hepatitis C and treatment failure: a genome-wide association study. *Gastroenterology* 2010;**138**:1338–45.

10. **Tanaka Y,** Nishida N, Sugiyama M, *et al*. lambda-Interferons and the single nucleotide polymorphisms: a milestone to tailor-made therapy for chronic hepatitis C. *Hepatol Res* 2010;**40**:449–60.
11. **Thomas DL,** Thio CL, Martin MP, *et al*. Genetic variation in IL28B and spontaneous clearance of hepatitis C virus. *Nature* 2009;**461**:798–801.
12. **Grebely J,** Petoumenos K, Hellard M, *et al*. Potential role for interleukin-28B genotype in treatment decision-making in recent hepatitis C virus infection. *Hepatology* 2010;**52**:1216–24.
13. **Thompson AJ,** Muir AJ, Sulkowski MS, *et al*. Interleukin-28B polymorphism improves viral kinetics and is the strongest pretreatment predictor of sustained virologic response in genotype 1 hepatitis C virus. *Gastroenterology* 2010;**139**:120–29.
14. **Layden-Almer JE,** Layden TJ. Viral kinetics in hepatitis C virus: special patient populations. *Semin Liver Dis* 2003;**23**(Suppl. 1):29–33.
15. **Heckel JL,** Sandgren EP, Degen JL, *et al*. Neonatal bleeding in transgenic mice expressing urokinase-type plasminogen activator. *Cell* 1990;**62**:447–56.
16. **Rhim JA,** Sandgren EP, Degen JL, *et al*. Replacement of diseased mouse liver by hepatic cell transplantation. *Science* 1994;**263**:1149–52.
17. **Tateno C,** Yoshizane Y, Saito N, *et al*. Near completely humanized liver in mice shows human-type metabolic responses to drugs. *Am J Pathol* 2004;**165**:901–12.
18. **Mercer DF,** Schiller DE, Elliott JF, *et al*. Hepatitis C virus replication in mice with chimeric human livers. *Nat Med* 2001;**7**:927–33.
19. **Tsuge M,** Hiraga N, Takaishi H, *et al*. Infection of human hepatocyte chimeric mouse with genetically engineered hepatitis B virus. *Hepatology* 2005;**42**:1046–54.
20. **Kurbanov F,** Tanaka Y, Chub E, *et al*. Molecular epidemiology and interferon susceptibility of the natural recombinant hepatitis C virus strain RF1_2k/1b. *J Infect Dis* 2008;**198**:1448–56.
21. **Kurbanov F,** Tanaka Y, Matsuura K, *et al*. Positive selection of core 70Q variant genotype 1b hepatitis C virus strains induced by pegylated interferon and ribavirin. *J Infect Dis* 2010;**201**:1663–71.
22. **Inoue K,** Umehara T, Ruegg UT, *et al*. Evaluation of a cyclophilin inhibitor in hepatitis C virus-infected chimeric mice in vivo. *Hepatology* 2007;**45**:921–8.
23. **Livak KJ,** Schmittgen TD. Analysis of relative gene expression data using real-time quantitative PCR and the 2(-Delta Delta C(T)) method. *Methods* 2001;**25**:402–8.
24. **Silver N,** Best S, Jiang J, *et al*. Selection of housekeeping genes for gene expression studies in human reticulocytes using real-time PCR. *BMC Mol Biol* 2006;**7**:33.
25. **Dahari H,** Layden-Almer JE, Perelson AS, *et al*. Hepatitis C viral kinetics in special populations. *Curr Hepat Rep* 2008;**7**:97–105.
26. **Neumann AU,** Lam NP, Dahari H, *et al*. Hepatitis C viral dynamics in vivo and the antiviral efficacy of interferon-alpha therapy. *Science* 1998;**282**:103–7.
27. **Honda M,** Sakai A, Yamashita T, *et al*. Hepatic ISG expression is associated with genetic variation in interleukin 28B and the outcome of IFN therapy for chronic hepatitis C. *Gastroenterology* 2010;**139**:499–509.
28. **Urban TJ,** Thompson AJ, Bradrick SS, *et al*. IL28B genotype is associated with differential expression of intrahepatic interferon-stimulated genes in patients with chronic hepatitis C. *Hepatology* 2010;**52**:1888–96.
29. **Dill MT,** Duong FH, Vogt JE, *et al*. Interferon-induced gene expression is a stronger predictor of treatment response than IL28B genotype in patients with hepatitis C. *Gastroenterology* 2011;**140**:1021–31.
30. **Hiraga N,** Abe H, Imamura M, *et al*. Impact of viral amino acid substitutions and host interleukin-28b polymorphism on replication and susceptibility to interferon of hepatitis C virus. *Hepatology* 2011;**54**:764–71.

Journal of Medical Virology 84:587–595 (2012)

Multiple Intra-Familial Transmission Patterns of Hepatitis B Virus Genotype D in North-Eastern Egypt

Mostafa Ragheb,[1] Abeer Elkady,[2] Yasuhito Tanaka,[2]* Shuko Murakami,[2] Fadia M. Attia,[3] Adel A. Hassan,[1] Mohamed F. Hassan,[1] Mahmoud M. Shedid,[1] Hassan B. Abdel Reheem,[1] Anis Khan,[2] and Masashi Mizokami[4]

[1]*Department of Endemic and Infectious Disease, Suez Canal University, Ismailia, Egypt*
[2]*Department of Virology and Liver Unit, Nagoya City University Graduate School of Medical Sciences, Kawasumi, Mizuho, Nagoya, Japan*
[3]*Department of Clinical Pathology Faculty of Medicine, Suez Canal University, Ismailia, Egypt*
[4]*Research Centre for Hepatitis and Immunology, International Medical Centre of Japan Konodai Hospital, Tokyo, Japan*

The transmission rate of intra-familial hepatitis B virus (HBV) and mode of transmission were investigated in north eastern Egypt. HBV infection was investigated serologically and confirmed by molecular evolutionary analysis in family members (N = 230) of 55 chronic hepatitis B carriers (index cases). Hepatitis B surface antigen (HBsAg) and hepatitis B core antibody (anti-HBc) prevalence was 12.2% and 23% among family members, respectively. HBsAg carriers were prevalent in the age groups; <10 (16.2%) and 21–30 years (23.3%). The prevalence of HBsAg was significantly higher in the family members of females (19.2%) than males (8.6%) index cases ($P = 0.031$). HBsAg and anti-HBc seropositive rates were higher significantly in the offspring of females (23%, 29.8%) than those of the males index cases (4.3%, 9.8%) ($P = 0.001$, 0.003), as well as higher in the offspring of an infected mother (26.5, 31.8%) than those of an infected father (4.7%, 10.5%) ($P = 0.0006$, 0.009). No significant difference was found in HBsAg seropositive rates between vaccinated (10.6%) and unvaccinated family members (14.8%). Phylogenetic analysis of the preS2 and S regions of HBV genome showed that the HBV isolates were of subgenotype D1 in nine index cases and 14 family members. HBV familial transmission was confirmed in five of six families with three transmission patterns; maternal, paternal, and sexual. It is concluded that multiple intra-familial transmission routes of HBV genotype D were determined; including maternal, paternal and horizontal. Universal HBV vaccination should be modified by including the first dose at birth with (HBIG) administration to the newborn of mothers infected with HBV. ***J. Med. Virol. 84:587–595, 2012.*** © 2012 Wiley Periodicals, Inc.

KEY WORDS: HBV genotype D; intra-familial transmission; vaccine

INTRODUCTION

Chronic hepatitis B virus (HBV) infection is a major health problem worldwide and is affecting approximately 350 million individuals [Lee, 1997]. Infection with HBV may lead to chronic state of hepatitis in 5–10% of patients who acquired the infection in the adult life and in 80–90% of patients who acquired the infection in the infancy [Chen, 1993]. Infection with HBV can lead to a progressive liver disease including liver cirrhosis and hepatocellular carcinoma (HCC) with approximately 1 million HBV-associated deaths from HCC every year [Seeger and Mason, 2000; Kao and Chen, 2002].

Based on the proportion of the population who are seropositive for hepatitis B surface antigen (HBsAg),

Grant sponsor: The Grant for National Center For Global Health and Medicine; Grant number: 22A-9; Grant sponsor: Grant-in-Aid for Japan Society for the Promotion of Science (JSPS) Fellows; Grant number: 21.09355.

Mostafa Ragheb and Abeer Elkady contributed equally to this study.

*Correspondence to: Yasuhito Tanaka, MD, PhD, Department of Virology and Liver Unit, Nagoya City University Graduate School of Medical Sciences, Kawasumi 1, Mizuho, Nagoya 467-8601, Japan. E-mail: ytanaka@med.nagoya-cu.ac.jp

Accepted 19 December 2011
DOI 10.1002/jmv.23234
Published online in Wiley Online Library (wileyonlinelibrary.com).

the world is divided conceptually into zones of high, intermediate, and low HBV endemic areas [Lavanchy, 2004]. In countries where the HBV infection is endemic, most infections result from the vertical transmission from the mother to the child in the peripartum period or from the infection in the early childhood. In the low HBV endemic regions, the neonatal or the childhood HBV infection is rare or even sporadic and the transmission of HBV occurs primarily among unvaccinated adults through the sexual transmission and injecting drug use [Custer et al., 2004].

Patients with chronic hepatitis B are considered to be the major reservoirs for the transmission of HBV. High incidence of infection with HBV is observed within the household contacts of chronic HBV carriers and it is not rare to have several members of the same household who have evidence of infection with HBV [Milas et al., 2000; Thakur et al., 2002]. However, the precise mechanisms of intra-familial spread have not been established clearly.

Different prophylactic strategies for controlling the HBV infection have been used by different countries depending on the prevalence of the HBV infection in each country [Poland and Jacobson, 2004]. The widespread immunization program against hepatitis B, which was implemented in more than 100 countries, was capable of dramatic reduction in the occurrence of chronic HBV infection and HCC [Zuckerman, 1997]. In Egypt, the HBV vaccine was included in 1992 in the Expanded Program of Immunization with injection at 2, 4, and 6 months of age [El Sherbini et al., 2006]. This program resulted in a significant reduction in the rate of acute symptomatic hepatitis B among the children in the age group eligible to receive the vaccine [Zakaria et al., 2007].

At least eight HBV genotypes have been identified based on the divergence of 8% or more of the entire nucleotide sequence and most of the HBV genotypes have a distinct geographical distribution [Okamoto et al., 1988; Norder et al., 1994; Stuyver et al., 2000]. Accumulated evidences indicated the difference in the virological characteristics among different HBV genotypes, which is reflected by the difference in the clinical outcome of infection with hepatitis B according to the infecting genotype [Miyakawa and Mizokami, 2003; Schaefer, 2005; Ozasa et al., 2006; Sugiyama et al., 2006]. However, data regarding the specificity of the transmission routes of each genotype is still scarce globally and need to be clarified.

The prevalence of HBV ranges between 2% and 6% in Egypt with the predominance of infection with HBV genotype D [Zekri et al., 2007]. It is widely known that Egypt is one of the countries with highest prevalence rate of infection with HCV in the world [el-Zayadi et al., 1992; Arthur et al., 1993; el Gohary et al., 1995]. However, the burden of HBV related progressive liver disease including liver cirrhosis and HCC in Egypt is observable either single or in a dual infection with HCV [Abdel-Wahab et al., 2000; el-Zayadi et al., 2005].

This study aimed to evaluate the prevalence of infection with HBV within the families of chronic HBV carriers in north Eastern Egypt. In addition, the intra-familial mode of transmission of HBV genotype D was also examined in the current cohort by the molecular evolutionary analyses. The impact of the HBV immunization programme in protecting this high-risk group was also investigated.

PATIENTS AND METHODS

Patients

The present study was conducted between January 2008 and June 2008 at the Communicable Disease Research and Training Centre, in Suez city. The study protocol was approved by the ethics committees of the participating institution and an informed consent was obtained from the included subjects.

Chronic HBV carriers were defined as individuals whose serum samples tested positive for HBsAg for at least 6-months period. Patients who fulfilled the criteria of chronic HBV carriers and were first detected within their families, were defined as the index cases (n = 55). The index cases included 40 (72.7%) men and 15 (27.3%) women. Their mean age (± SD) was 41 ± 10.7 years and all the index cases were negative for HBeAg.

A total of 230 household contacts of the index cases were included in the study and defined as family members group. Data regarding their family relationship to the index cases, age, and the HBV vaccination history have been obtained.

According to the kinship of the family members to the index case group, the family members included 139 offspring, 4 parents, 46 spouses, 15 siblings, and 26 defined as other relatives who are living in the same house with the index cases.

Serological Methods

Serum samples were collected from the index cases and family members groups.

The Serum samples were examined for HBsAg, anti-HBc, anti-HBs, and HBeAg by the chemiluminescence enzyme immunoassay with the commercial assay kits (Fujirebio, Inc., Tokyo, Japan). The examination of the serum samples for anti-HCV and HIV was conducted using commercial kits (Abbott Laboratories, Abbott Park, IL).

Molecular Evolutionary Analysis

The HBV/DNA was extracted from 200 μl of serum samples positive for HBsAg using the QIAamp DNA MiniKit (QIGEN, Inc., Hilden, Germany), and re-suspended in 100 μl of a storage buffer (provided by the kit manufacturer).

The entire preS2 and S regions of the HBV genome (799 nucleotides; nucleotide positions 34–833) were amplified using the primers set and the conditions described previously [Sugauchi et al., 2001].